# *Chapter 2*

## *β-cyclodextrin based dual-responsive multifunctional nanotheranostics for cancer cell targeting and dual drug delivery*

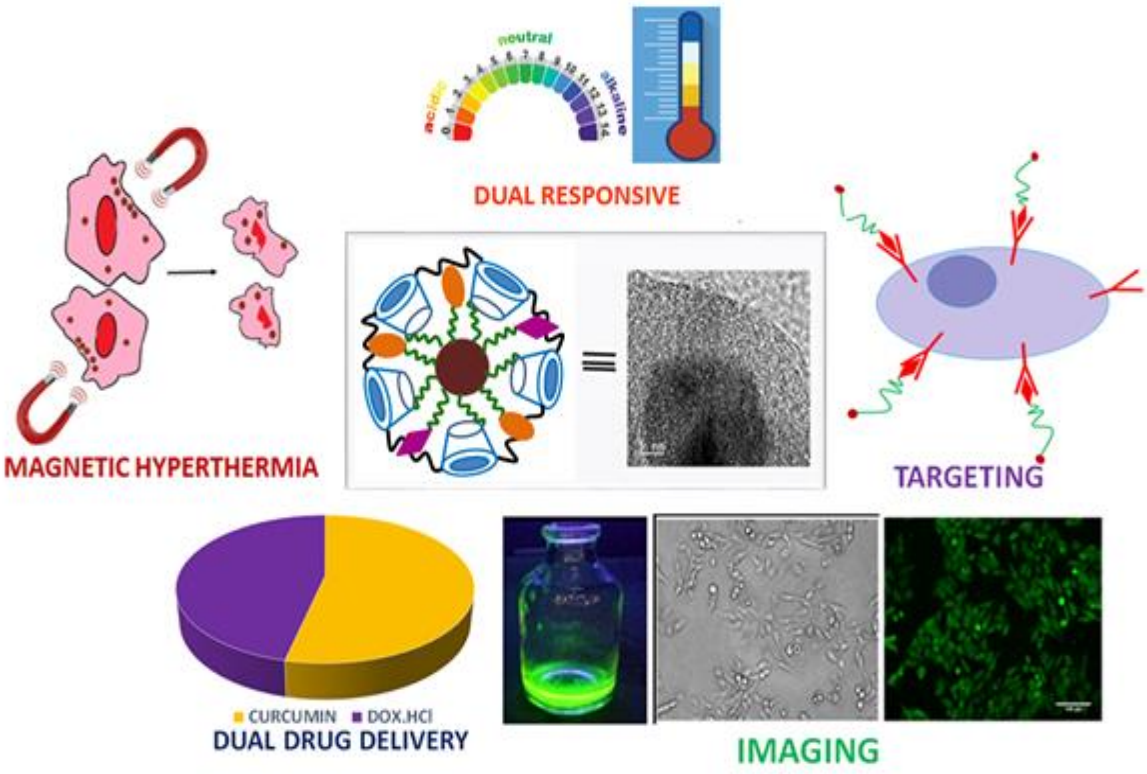


**Published in *Carbohydrate Polymers*, 2019, *206*, 694-705**

## 2.1 Introduction

Chemotherapy, the main stray in the treatment of malignancies, employs chemical agents to destroy cancer cells. Due to lack of selectivity, such chemical agents destroy healthy cells along with cancerous cells, inviting a serious drawback of adverse side effects and lowered therapeutic effect [1]. Additionally over the course of therapy drug resistance may occur either due to lack to targeted drug delivery to tumor site or due to genetic alterations of the cancer cells[2]. Targeted delivery of chemotherapeutic drugs specifically towards cancer cells is one of the apparent solutions to overcome the limitations of selectivity. On the other hand drug resistance and mutations induced by drugs may be overcome with the help of combination chemotherapy wherein combination of two or more drugs is employed which disrupts different stages of the cell and enhances the apoptosis of cancer cells [3].

The design of an efficient drug delivery system, which targets drugs specifically to tumor site with improved therapeutic efficacy and minimal side effects, is a challenge for cancer therapy. Bearing this fact in mind, the concept of engineering multifunctional materials possessing more than one useful property in the same system, have been proposed for the evolution of targeted drug delivery system. Further, the amalgamation of imaging and therapeutic capabilities on a single nanoplatform, resulting in an approach termed "theranostics", has been recently realized and has gained increasing attention for drug delivery monitoring, image-guided therapy and therapy response observation[4]. Stimuli-responsive polymers that upon exposure to specific environmental stimuli, such as changes in temperature, pH value, light, ionic strength, or magnetic field, undergo reversible changes in microstructure are often employed.

In the light of this approach in the past few years, efforts have been directed towards development of multifunctional materials for cancer therapy. They are based on magnetic nanoparticles, Graphene, Mesoporous Silica, Carbon Nanotubes, carbon[5] and gold nanoparticles. Many of these materials serve as core for a polymer shell (silica-polymer, Gold-polymer) [5,6]. Among stimuli responsive polymers Poly-N-Isopropyl acrylamide (PNIPAM) is widely explored polymer for including temperature response, and possibility of reversible aggregation and dispersion of PNIPAM coated nanoparticles. The thermal response is beneficial to monitor specific targeting of cancer cells due to temperature gradient of normal cells (37°C) from cancerous cells (43°C).

Magnetic nanoparticles (MNPs) are popularly adopted in the biomedical field due to their response to external magnetic field for easy magnet driven transport and hyperthermia therapy (Liu et al., 2016, Chen et al., 2017). Surface-functionalization of MNPs with of complimentary moieties can impart drug carrying efficiency with additional diagnostic and therapeutic benefits. β-Cyclodextrin (CD), a torus shaped non-toxic cyclic oligosaccharide, with a hydrophobic cavity inside and a hydrophilic region in the outer surface and is found to be most suitable for the inclusion binding of appropriately sized guest compounds. The inclusion complex of drug molecules with CD enhances its bioavailability, solubility and stability. β-Cyclodextrin (CD) can be covalently conjugated to MNPs. The use of CD opened up the frontiers for dual drug loading which can be exploited for use in combination chemotherapy. Firstly, CD can form inclusion complex with drug (Hu, Tang, & Chu, 2014, [10]. Secondly being a multi-hydroxyl compound it can form crosslinked network and the drug molecules can get entrapped within such polymeric matrix (Eid et al., 2011, A. R. Solanki, Kamath, & Thakore, 2015).

We have successfully synthesized β-cyclodextrin-magnetic nanocarriers using diisocyanate as a linker which exhibited intriguing capabilities to carry high drug payload as well as controlled drug release[13]. Diisocyanate is extremely reactive towards hydroxyl as well as amine groups. Encouraged by these observations, we aimed to introduce stimuli responsive moieties with cancer-targeting ligand like folic acid and fluorescent label in magnetic nanoconjugates by virtue of isocyanate/urea linkage. Urethane and urea formation proceed quite easily and all functionalities can be introduced in a single step (one pot synthesis) (A. Solanki, Mehta, & Thakore, 2014 , A. Solanki, Das, & Thakore, 2018).

This has an advantage over most of the multifunctional theranostics which consist of basic architecture of silica around MNPs ($Fe_3O_4$@$SiO_2$) that restricts loading of hydrophobic drug. Several others involve complex synthetic steps which restrict their large scale generation.

The ultimate goal is simplified synthesis of multifunctional nanoconjugates with therapeutic and diagnostic capabilities equipped with features for targeted stimuli responsive release of multiple drugs with following features

1. Several β-cyclodextrin (CD) units to carry high payload of both hydrophilic and hydrophobic anticancer drugs and dual delivery for use in combination chemotherapy.
2. CD modified by Maleic anhydride and Poly (N-Isopropylacrylamide) (NIPAM) for pH and thermo-responsive drug release.

3. Fluorescein for monitoring cellular uptake.
4. Folic acid for targeted drug delivery.
5. Superparamagnetism for control of intracellular movements for final clearance from the body.

Curcumin and DOX.HCl were used as model drugs to assess the dual drug delivery by the nanoconjugates. Curcumin is a potent anticancer agent devoid of side effects but is hydrophobic in nature and hence has poor bioavailability [16]. Encapsulation in the hydrophobic cavity of cyclodextrin can enhance its bioavailability.

*In-vitro* investigations carried out using cancer and non-cancer cell lines established the utility of the materials for targeted delivery. Promising in-vitro performance of the materials were observed in terms of better internalization and corresponding cell death of a poorly available drug curcumin. The studies were further extrapolated to assess the performance of the nanoconjugates *in-vivo* with the results in agreement to *in-vitro* studies.

## 2.2 Experimental Section

### 2.2.1 Materials

β-Cyclodextrin, Maleic Anhydride, Iron oxide nanoparticles, Folic acid, Hexamethylene diisocyanate (HMDI), Curcumin, Doxorubicin Hydrochloride (DOX), N-Isopropylacrylamide (NIPAM) and N,N'-Methylene bisacrylamide (MBA) was purchased from Sigma Aldrich, India and used as received. Fluorescein was purchased from Loba Chemie. Dimethyl formamide (DMF) was purchased from Spectrochem India. Phosphate buffer saline tablets (for preparation of pH 7.4 buffer solution) were obtained from Sigma Aldrich, India. Glacial acetic acid, Sodium acetate (for preparation of acetate buffer solution) was procured from Sisco Research Laboratories (SRL), India.

### 2.2.2 Synthesis of nanoconjugates

The synthetic route followed for the preparation of the nanoconjugates is as per **scheme 2.1- 2.3**.

#### 2.2.2.1 Synthesis of CD-MA

For the synthesis dissolution of CD (500 mg) in DMF (25 ml) was carried out, later NaH (15 mg) was added into the solution via rapid stirring Stirring was continued for 6 h at room

temperature. Later on solid MA (50 g) was added to the solution wherein b-CD oxoanion is formed. The reaction mixture was continuously stirred in a sealed round bottom flask in an oil bath at a controlled temperature (100 °C) for 1 h. The reaction product was precipitated and washed with a large quantity of acetone, and finally dried to obtain a brown powder.

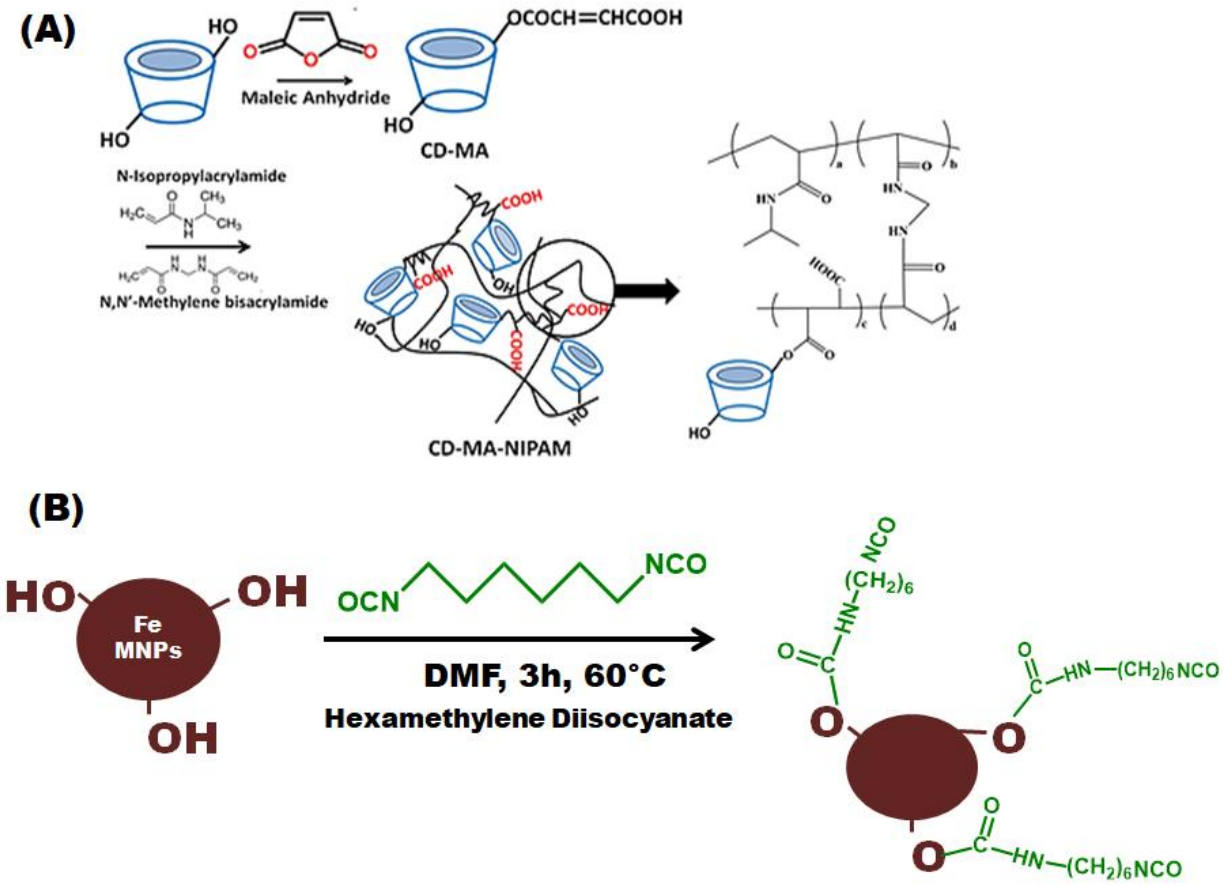


**Scheme 2.1: Synthesis of (A) cyclodextrin derived pH-thermal dual responsive polymer and (B) NCO functionalization of iron oxide nanoparticles.**

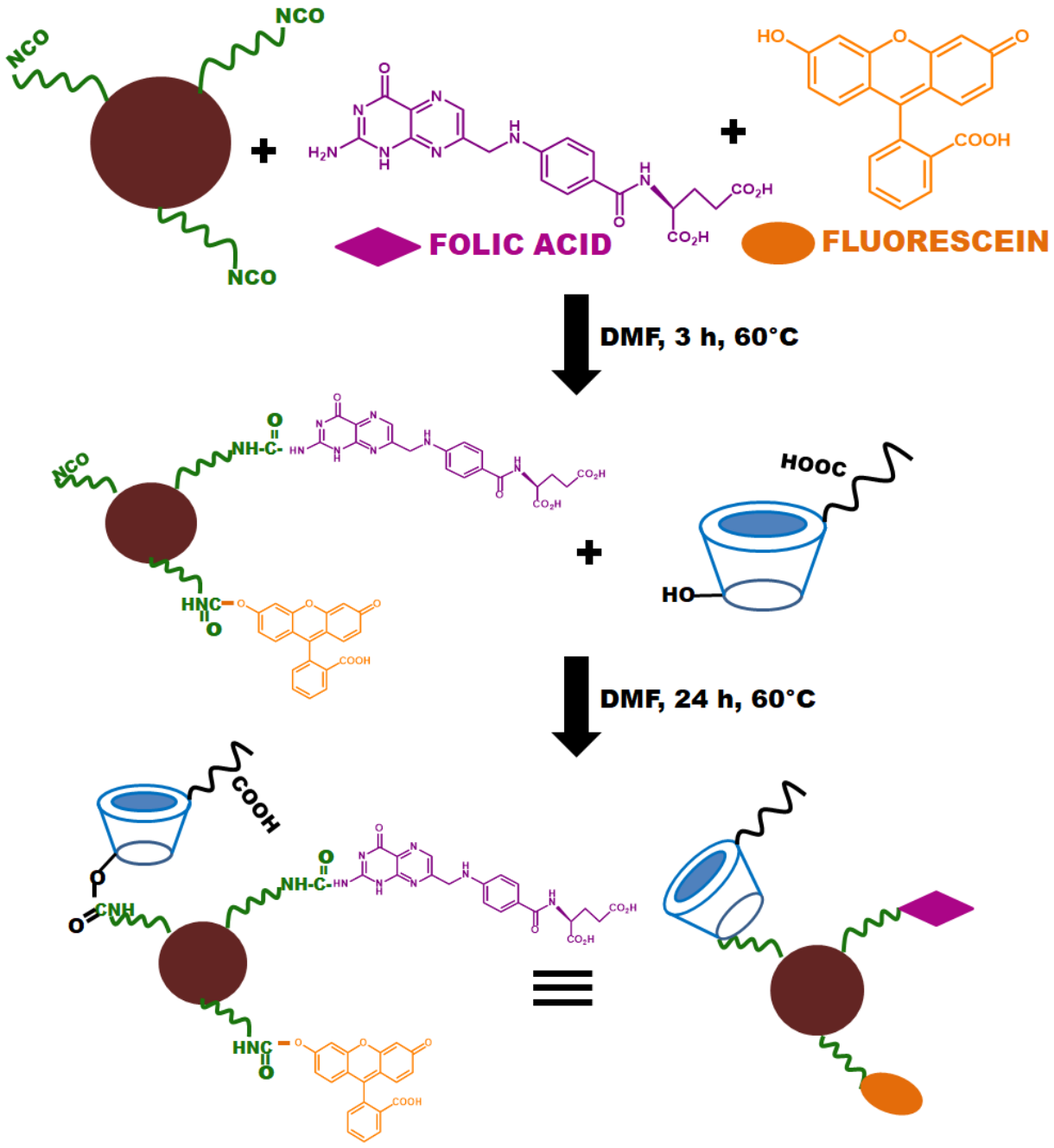


**Scheme 2.2: Synthesis of the multifunctional nanoconjugates**

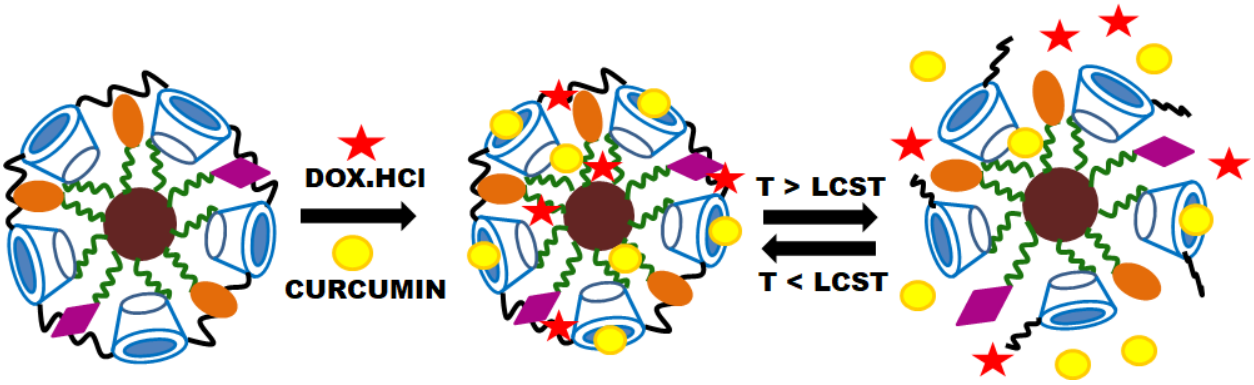


**Scheme 2.3: Schematic showing drug loading and release from the nanoconjugates**

### 2.2.2.2 Synthesis of CD-MA-NIPAM Copolymer

Polymerization of NIPAM (100 mg) and CD-MA (100 mg) was carried out by a precipitation polymerization method using in the presence of KPS (5 mg) (as an initiator) and MBA (40 mg) (as a cross-linker) under nitrogen atmosphere at 70 °C. The mixture was cooled to room temperature and resultant product was given washings of acetone.

### 2.2.2.3 One pot two step synthesis of multifunctional nanoconjugates

**Step-1:** Iron oxide nanoparticles (50 mg) were dispersed in 5 ml DMF by sonication. HMDI (0.5 g) was added to the solution mixture, the reaction was allowed to proceed at 60 ˚C for 3 hours. This resulted in isocyanate functionalization of MNPs.

**Step-2:** Fluorescein (52 mg) and Folic Acid (46 mg) was dissolved in 5 ml of DMF respectively and these solutions were added to the reaction mass slowly and drop wise during course of 15 minutes. The reaction was allowed to proceed for 3 hours at 60 ˚C. CD-MA-NIPAM co-polymer (65 mg) was dispersed in DMF was then added to the reaction mixture. The reaction was allowed to proceed at 60 ˚C for 24 hours. The product was isolated via decantation with an external magnet and purified by giving washings of water and acetone.

## 2.2.3 Characterization methods

The FTIR spectra were recorded as KBr discs on a Bruker IR spectrophotometer at room temperature. Energy dispersive X-ray (EDX) analysis of the sample was recorded by the model-JSM-5610 LV attached to Scanning electron microscopy (SEM). FEI (Technai G2, F30) electron microscope was used at an acceleration voltage of 300 kV to carry out High-Resolution Transmission Electron Microscopy (HR-TEM) analysis of the sample. Vibrating sample

magnetometer (VSM) analysis was carried out by using Lakeshore VSM 7410 at room temperature. UV-visible Spectrophotometer experiments were performed on Perkin Elmer Spectrophotometer, Inc, MA, USA and fluorescence data was recorded on JASCO FP-6300 spectrofluorometer. Variable temperature Dynamic Light Scattering measurements were performed on Beckman Coulter Delso Nano. Thermo gravimetric analysis (TGA) was carried out by using TG–DTA 6300 INCARP EXSTAR 6000 in the temperature range of 30–500°C and heating rate of 10°C/min. The nitrogen atmosphere was maintained throughout the measurement.

### 2.2.4 Preparation of drug loaded nanoconjugates

A batch loading technique was utilized for the encapsulation of curcumin on nanoconjugates [17]**.** Briefly, 5 mL of curcumin having 30 mg/mL concentration was obtained by dissolution of 150 mg drug in of 1:1 solution of water and ethanol. For encapsulation, 150 mg of carrier sample was dispersed in a vial having 5 mL of 30 mg/ml drug solution. This suspension was stirred under dark conditions overnight at room temperature The removal of drug loaded nanoconjugates from drug solution was done by using an external magnet. Washings of ethanol were given twice to ensure the removal of free drug. The drug-loaded nanoconjugates were then allowed to dry at room temperature for 24h and preserved in desiccators. The concentration of drug in supernatant was analyzed by calibration plot of curcumin prepared on UV-vis spectrophotometer at 430 nm. The drug entrapment efficiency (%LE) and drug loading content of nanoconjugates was quantified as per following equations [18], [19].

$$\%\ enrapment\ efficiency = \frac{Ic-Sc}{Ic} \times 100 \qquad \text{--- (1)}$$

Where $I_C$ is initial content of curcumin used and $S_C$ stands for concentration of curcumin in supernatant.

$$\%\ drug\ loading\ content = \frac{Weight\ of\ drug\ in\ nanoconjugates}{Weight\ of\ drug\ loaded\ nanoparticles} \times 100 \qquad \text{---- (2)}$$

DOX.HCl was loaded on the nanoconjugates using the similar protocol. The concentration of drug in the supernatant was determined with the help of a calibration plot prepared by UV-spectrophotometric determination of DOX at 480 nm.

The release experiments were performed using drug loaded nanoconjugates under varying pH conditions i.e. in PBS buffer (0.1 M, pH 7.4) and in Acetate Buffer (pH- 5.0) in an Erlenmeyer flask. The release was also monitored at two different temperatures 37 °C and 40 °C. For the study, 10 mg of drug loaded nanoconjugates were suspended in 25 mL of release medium and kept under constant stirring maintained at 37 °C/40 °C. The release media (3 mL) was periodically removed and same volume of the fresh release media was replenished each time. The content of drug released was determined using UV-vis spectrophotometer at 430 nm for curcumin and at 480 nm for DOX.HCl respectively.

### 2.2.5 Cell Culture and Cell Viability assay

Hela (Cervical Cancer Cell line) was procured from National Centre of Cell Sciences, Pune, India. Cells were maintained at 37 °C and 5% $CO_2$. Cells were seeded ($1\times10^5$ cells) in a T25 flask and cultured in DMEM containing 10% FBS and 1% antibiotic–antimycotic solution with trypsinization at every third day and sub-culturing with a TPVG solution.

Cell viability was evaluated by MTT (3-[4,5-dimethylthiazol-2- yl]-2,5-diphenyltetrazolium bromide, Sigma-Aldrich). Cells ($7\times10^3$ cells per well) were seeded in 96-well culture plates, allowed to grow overnight and treated with compounds to be analyzed at a dose range of 10- 500 µg/ml for 24h, then 100 µl of MTT was added to the wells and incubated for 4 h at 37°C. MTT solution was removed and the resultant formazon was dissolved in 150 µl of DMSO. The resulting absorbance was analyzed at 540 nm in and the cell viability percentage was quantified with respect to control. Experiment was also repeated by placing a circular magnet under the 96 well plates prior to MTT assay.

### 2.2.6 Hemolysis assay

Whole blood was collected from healthy human volunteer and hemolysis assay was performed. [20]. A prior consent followed and the protocol was approved by Indian medical association (IMA) for research on human subjects. All experiments were performed at Blue cross pathology lab (IMA-BMWMC no. 1093), Vadodara, India in compliance with laws and guidelines of IMA.

The samples of blood were collected in vacutainer tubes coated with ethylene diamine tetra-acetic acid (EDTA) and subjected to treatment with higher concentration (200µg/ml) of the nanoconjugates. Untreated sample was used as negative control as it showed 0% hemolysis on

the other hand, sample treated with distilled water showing 100% hemolysis) was employed as positive control. After incubation for 3 h the tubes were centrifuged at 1500 rpm for 10 min and photographed (Sony cybershot W830). The extent of Hemolysis was quantified using the following equation [21].

$$Hemolysis\ \% = \frac{As - Aneg}{Apos - Aneg} \times 100 \quad \text{---------- (3)}$$

In this equation $A_s$ represents absorbance of sample whereas $A_{pos}$ and $A_{neg}$ absorbance of positive control and negative control respectively.

### 2.2.7 Cellular Internalization

Hela cells were seeded in a 6 well plate and allowed to grow overnight. Later, Hela cells were dosed with nanoconjugates (200µg/ml) and incubated for 24 h. Cells were washed with PBS and observed for presence of fluorescence. Cells were photographed at 400X using Floyid cell imaging station (Life Technologies, USA). Experiment was repeated by placing a circular magnet under the 6 well plate prior observation and photography of cells.

### 2.2.8 Cell mortality assay

Cells were seeded in 12 well plate and incubated with the curcumin for 24 h. Later, cells were washed with PBS and 50µg/ml of Propidium iodide (PI) was added to the wells and incubated for 15 minutes at 37°C [22]. Cell death induced by the treatment of curcumin was observed and photographed at 400X using Floyid cell imaging station (Life Technologies, USA).

### 2.2.9 In-vivo studies for anticancer potential

Laboratory animals (Balbc mice 28-30 g n= 24, male/female) were procured from Zydus Research Center, Ahmedabad, India. Animals were housed under standard conditions of LD 12:12 with food and water ad libitium. Ethical clearance for animal experimentation was obtained from Institutional Animal Committee (IAEC) and CPCSEA. Experimental groups (n=6 per group) viz untreated equal to control, intraperitoneal injected with HEPG2 cells and allowed to develop hepatic tumor (HCC), HCC animals treated with Doxorubicin (DOX), and HCC animals treated with nanoconjugates loaded with DOX (DOX+NC) were used for the study.

HCC and HCC+NC were also injected intraperitoneally. The experiment continued for 15 days and at the end, body weights were recorded. Blood was collected by retro-orbital sinus puncture and serum was separated in cold centrifuge (3000 rpm). Hepatic markers for liver function (SGPT and SGOT) were assessed using standard kits (Reckon diagnostics Ltd., Vadodara, India). Inflammatory markers in serum (TNF-α, IL-6, IL-10, IL-12 IFN-α and MCP-1), markers of matrix modulation (MMP-2 and 9), and serum markers of HCC (AFP) were assessed by ELISA kits (Krishgen Biosystems, Mumbai, India). Animals were sacrificed under mild ether anesthesia and liver autopsy was conducted. Pieces of liver tissue obtained from control and experimental groups were stored in RNA later solution. Forward and reverse primers of genes controlling immunity (TLR-2 and 4) were procured from Eurofins Scientific, New Delhi, India. RNA extraction was done by Trizol reagent and cDNA was synthesized using iscript$^{TM}$ cDNA kit (BIORAD, California, USA). Quantitative RT-PCR was performed using SYBR select master mix (Applied Biosystems in Quant Studio 12 K (Life Technologies) real time PCR machine.

## 2.3 Results and discussion

### 2.3.1 Synthesis of nanoconjugates

The synthesis of the fluorescent nanoconjugates was done in a one pot 2 step method as outlined in Scheme 1. The first step includes the preparation of CD-MA-NIPAM copolymer. The second step includes functionalization of surface hydroxyl groups of MNPs with isocyanate functionalities of Hexamethylene Diisocyanate (HMDI) [23],[24]. The addition of fair excess of HMDI ensures sufficient free NCO groups, which can be employed for linking of the required functionalities on the surface of the MNPs. The third step includes introduction of the fluorophore Fluorescein (FL) and the targeting ligand Folic acid (FA). The hydroxyl group of FL and amino groups of FA form covalent bonds with isocyanate group of HMDI (Zhang et al., 2012). Remaining free NCO groups of HMDI are utilized to form urethane linkage with the hydroxyl groups of CD-MA-NIPAM copolymer [26].

### 2.3.2 Characterization of nanoconjugates

The starting materials were scanned using FTIR spectroscopy **(Figure 2.1A)**. The successful assortment of all the required functionalities was confirmed by the presence of relevant functional groups in the FTIR spectra. The FTIR spectra **(figure 2.1B)** were recorded after each

synthetic step in order to ascertain the formation of the required material and their subsequent conjugation to form the final material. The IR spectra of CD-MA polymer show characteristic peaks of hydroxyl groups at 3347 $cm^{-1}$ confirming the presence of cyclodextrin moieties [27]. The appearance of peak at 1725 $cm^{-1}$ indicates the presence of carbonyl groups which is due to the polymerization of maleic anhydride with cyclodextrin [28]. The strong band appearing at 665 $cm^{-1}$ shows the presence of C=C groups which was further anticipated to react with the double bond of NIPAM to form a new crosslinked polymer CDMA-NIPAM (ref). The spectra of CDMA-NIPAM shows peaks at 2971-2876 $cm^{-1}$ corresponding to the presence of isopropyl groups, the strong peak for C=O amide group appears at 1640 $cm^{-1}$ and that corresponding to NH amide group is observed at 1540 $cm^{-1}$ (Bafkary & Khoee, 2016).

A broad secondary amine (NH) peak at 3291 $cm^{-1}$ corresponds to the characteristic poly (NIPAM) bands [30]. This confirms the formation of the new dual responsive polymer.

The FTIR spectra of the nanoconjugates peaks corresponding to Fe-O linkage of MNPs was observed at 599.47 $cm^{-1}$ corresponding to Fe-O bonds for MNPs [31]. The single broad band at 3330.57 $cm^{-1}$ relate to the OH groups of β-cyclodextrin, while other peak at 1620.44 $cm^{-1}$ indicates C=O stretching frequency. The peak at 1563.77 $cm^{-1}$ corresponds to N-H and C-N groups in the urethane linkage. This confirms successful conjugation of the dual responsive polymer with surface hydroxyl groups MNPs [32].

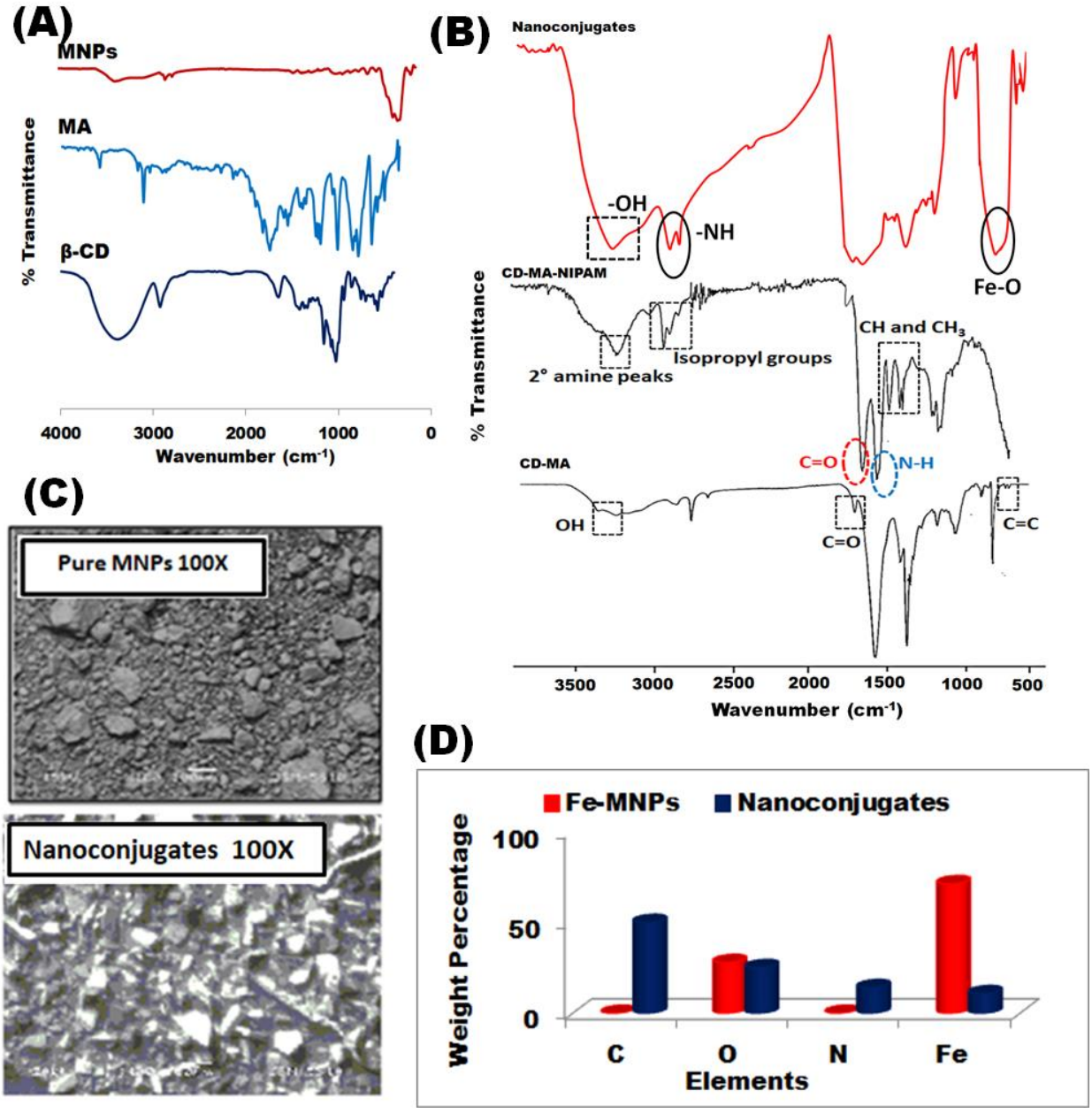


**Figure 2.1: FTIR spectra overlay of (A) starting materials (B) polymers and nanoconjugate; (C) comparison in SEM images (D) elemental analysis of bare FeMNPs and nanoconjugates**

The bands at 2857.12 $cm^{-1}$ and 2928.40 $cm^{-1}$ corresponds to N-H stretching frequencies, which confirms the conjugation of folic acid. The peaks at 1111.88 $cm^{-1}$ showing C-O stretching

frequency and 768.86 $cm^{-1}$ that appears due to C-H bending frequency suggests successful conjugation of fluorescein (Zhang et al., 2012).

The morphology of nanoconjugates was observed using SEM and compared with the morphology of bare iron oxide nanoparticles as shown in **figure 2.1C**. The nascent $Fe_3O_4$ nanoparticles by virtue of their nano-size appear as aggregated particles. Introduction of chemical conjugations on the surface of these nanoparticles results in an increase in the size, which is evident from the images [33]. The elemental composition of pristine MNPs was composed of 71.33% of Fe and 27.95% of O **(Figure 2.1D)**. However, the elemental composition of the nanoconjugates showed presence of elemental carbon, and nitrogen in addition to presence of Fe and O. This evidence indicates a conjugation of various organic moieties on the surface of MNPs.

Further, the successful conjugation of fluorescein was confirmed with the help of UV-Visible spectrophotometric and spectroflourometric determination **(figure 2.2A&B)**. The nanoconjugates exhibited excellent fluorescent properties in water supported by a broad absorbance band ranging from 490 to 580 nm with emission maxima at 520 nm [34]. The inset images display an intense green fluorescence of the nanoconjugate sample dispersed in water.

HR-TEM images as observed in **Figure 2.2C** depict size distribution of pure $Fe_3O_4$ as well as nanoconjugates and the results are in good agreement with SEM micrographs. Bare MNPs were observed as small nanoparticle aggregates. It was observed that the nanoconjugates demonstrated spherical shape and were discrete, showing monodispersity and narrow size distribution. MNPs showed a size range of 20-25nm and nanoconjugates (55-65 nm) suggests that the thickness of polymer layer might be approximately 35- 40 nm. This, once again, suggests successful conjugation of dual responsive polymer on the surface of nanoparticles.

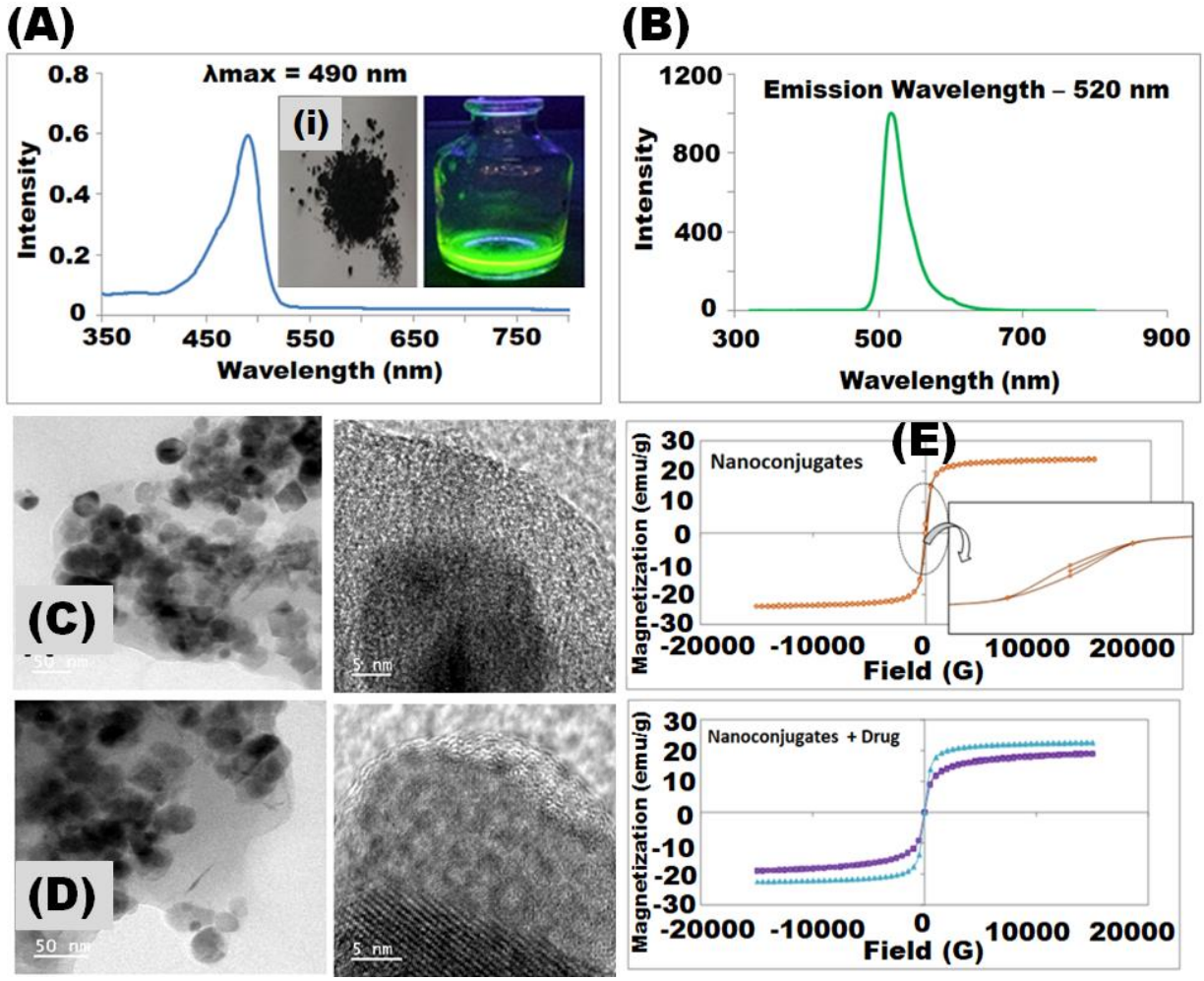


**Figure 2.2: Optical properties of the nanoconjugates as shown by (A) UV-Vis spectra (B) fluorescence spectra (i) inset photographs showing image of nanoconjugates under normal light and upon emission of photoluminescence by UV irradiation HR-TEM images of multifunctional nanoconjugates (C) before drug loading and (D) after drug loading. Room temperature magnetization curves of (E) pristine nanoconjugates and comparison of magnetization for pure as well as drug loaded nanoconjugates.**

Moreover the contrast in the images shows that these nanoconjugates have a core-shell structure. The darker region contrast corresponds to the metallic magnetic core and the lighter contrast is due to polymeric shell [35].

Since the nanoconjugates were prepared using iron oxide nanoparticles as the platform for functionalization making them magnetic in nature. This gives the advantage of influencing the

movement of the particles inside the body using an externally applied magnetic field. For an effective control over the movement of the particles, the magnetic force applied externally must be able to overcome the hemodynamic force of the bloodstream. For desirable in-vivo applications low magnitude of magnetic field needs to be applied and hence material with high magnetization are desired [36].

The magnetic properties of the nanoconjugates were assessed using Variable Sample Magnetometer (VSM). The hysteresis loops obtained for nanoconjugates prior to and post drug loading are demonstrated in **Figure 2.2E**. The coercivity, retentivity and magnetization value for nanoconjugates is 3.5591 G, 424.59 emu and 97.65 emu respectively.

The high values of magnetization obtained for our samples make them suitable for in-vivo applications. For drug loaded nanoconjugates the values are 79.634, 17.128 and 0.143 for coercivity, retentivity and magnetization values respectively.

A decrease in the magnetization value of drug loaded nanoconjugates was observed which can be attributed to presence of drug molecules on the surface [32]. This confirms successful loading of drug on the nanoconjugates. Moreover the nanoconjugates exhibit a ferromagnetic behavior which could be confirmed with the help of an external magnet. The particles dispersed in water were easily attracted to the wall of the glass vial where external magnet was placed. These results thus confirm that the conjugation of the polymer on the surface of MNPs does not affect the super-paramagnetism of the iron oxide nanoparticles.

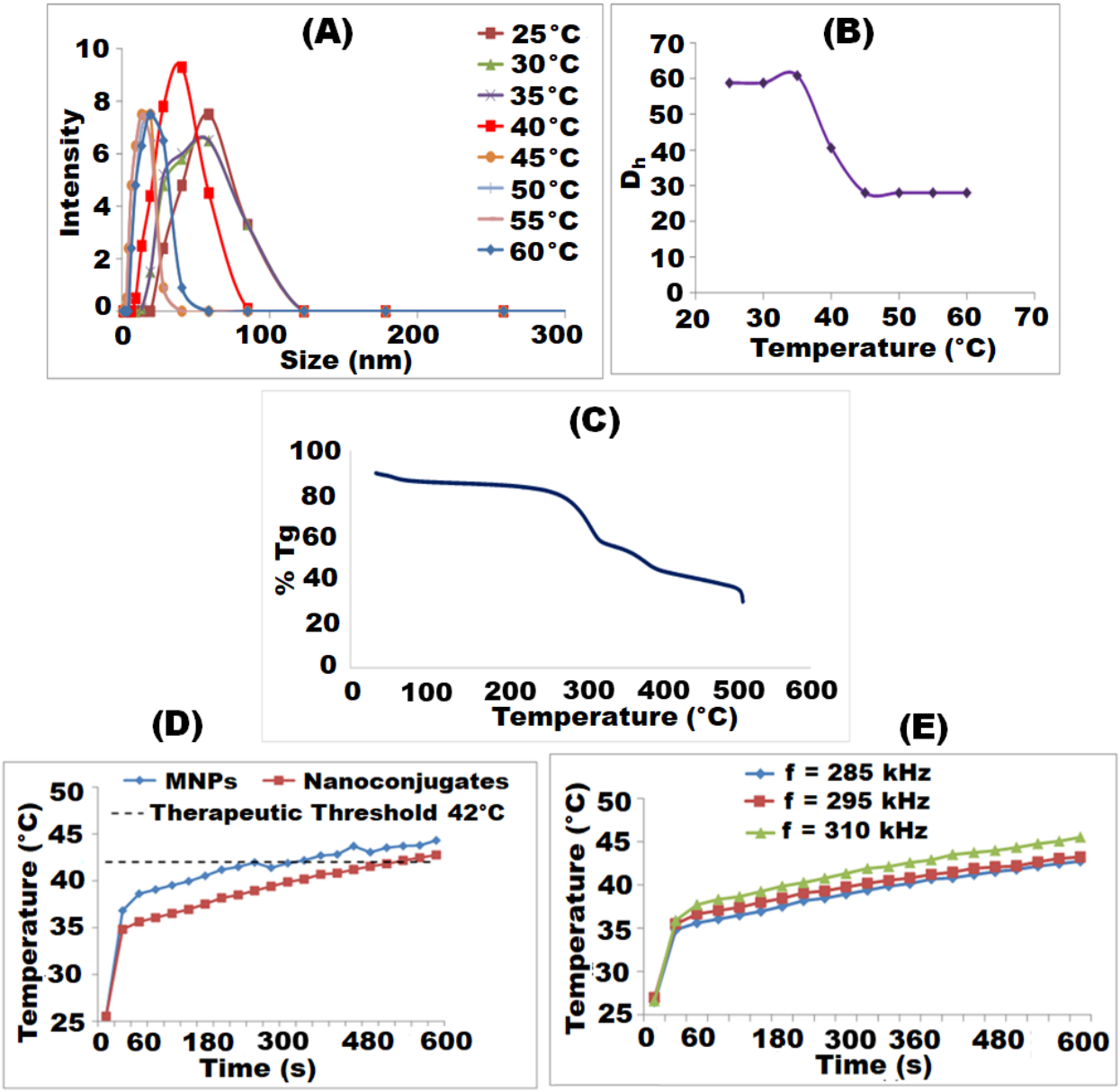


**Figure 2.3: Plot of (A) variable temperature DLS histograms of nanoconjugates in water (1.0 mg/mL) and (B) hydrodynamic diameter of nanoconjugates (1.0 mg/ mL) as function of temperature in water (C) TGA plot of the nanoconjugates Magnetic Hyperthermia studies, graph of (D) temperature versus time comparing the heating efficiencies of pure iron oxide nanoparticles and nanoconjugates at a concentration of 1 mg/ml at 285 kHz frequency and (E) Comparison of heating efficiencies of nanoconjugates at a concentration of 1 mg/ml at various frequencies.**

The thermo-responsiveness of the nanoconjugates was investigated by variable temperature DLS measurements **(Figure 2.3A & B)**. The size of the particles varied with the change in temperature. At 25°C, the hydrodynamic diameter of the multifunctional nanoconjugates was 59 nm; the particles are monodispersed which is in agreement with the data of HR-TEM. The size of the nanoconjugates decreases at 40 °C, the hydrodynamic diameter of the nanoconjugates changed to 40 nm. The diameter of the particles decreases as a result of the dehydration of polymer chains and collapse of the hydrophilic segments of PNIPAM above the transition temperature.

These results provided evidence for thermosensitivity of the nanconjugates and that the thermal response of NIPAM is retained even after covalent conjugation with CD-MA.

The nanoconjugates were analyzed with TGA **(figure 2.3C)** for the determination of thermal properties. A degradation of 4.9 % below 200° C is due to the loss of water molecules adsorbed (Solanki and Thakore et al., 2015). The second stage of degradation of about 27.2% in the temperature range of 200°C to 350°C occurs due to the breaking of urethane linkages which corroborates with carbohydrate based polyurethanes which undergo degradation at around 200°C temperature [12]. The degradation on the region of 360°C to 500 °C may be due CD molecules undergoing decomposition [38].

### 2.3.3 Magnetic Hyperthermia Studies

The use of superparamagnetic iron oxide ($Fe_3O_4$) nanoparticles as a backbone of nanoconjugates make them potential agents for hyperthermia treatment of cancer [39]. Magnetic Hyperthermia (MH) is a therapeutic procedure wherein the temperature of the area affected by cancer is increased by the application of magnetic particles using irradiation by an external alternating magnetic field [40]. The cancer cells die at a temperature of about 43 °C, since their oxygen supply by the blood vessels is not sufficient. On the contrary, normal cells are not damaged at even higher temperatures. The heating during MH occurs because energy is absorbed by the magnetic nanoparticles upon irradiation with a low-frequency (i.e.100 kHz–900 kHz) alternating magnetic field (AMF). The particles then transform the energy of the magnetic field into heat via different physical mechanisms [41]. The graph of temperature vs. time of the suspension of nanoconjugates showed a gradual increase in temperature under AC magnetic fields. As shown in **Figure 2.3D & E**, it was observed that a magnetic field of frequency 285 kHz is capable of producing energy

which raises the temperature of the suspension of 1 mg/ml of nanoconjugates to 40-45 °C within 20 minutes. The field depended study was conducted, revealed that with increase in field strength, less time is required to heat the solution up to 40-45 °C.

### 2.3.4 Drug loading and release studies

The drug entrapment efficiency of the nanoconjugates was 88%. The drug loading content was found to be 45 wt% for curcumin and 32 wt% for DOX. This can be explained as follows. Because of the hydrophobic nature, curcumin gets encapsulated in the cavity of cyclodextrin in addition to entrapment in the polymeric matrix. The hydrophilic nature of DOX does not facilitate its entry in the cavity of cyclodextrin, so it is encapsulated only within the polymeric matrix. The release was investigated in phosphate buffer saline at pH 7.4 and acetate buffer pH 5.0 at 37°C (physiological pH) and at elevated temperature 40°C, which is the transition temperature for the thermoresponsive polymer. All the studies were performed in triplicate and drug release study plots were constructed using the mean values. A slow and sustained release is observed for both the drugs over the period of study. The release profiles showed that release rates are depended on both pH as well as temperature.

For the release of DOX, it was observed that almost 60% of the loaded drug was released at pH 5 and 37 °C, but more than 80% release was observed at pH 5 and 40 °C (figure 4). Thus it can be said that superlative release of DOX could be obtained under acidic pH conditions and elevated temperature, which coincides with the tumor microenvironment. The drug release is attributed to chemical structure of drug and its interaction with polymeric chains on the surface of nanoconjugates. DOX holds positively charged protons on its structure. At pH 7.4, positively charged DOX molecules interact with negatively charged polymer chains due to electrostatic forces of attraction. This results into higher adhesion of drug molecules on the nanoconjugates, resulting into slower diffusion of drug molecules. On the contrary, under acidic conditions, the carboxylic acid groups of the polymer undergo protonation which weakens the electrostatic interaction, leading to easy diffusion of drug molecules, as well as shrinkage of polymer. This results into enhanced DOX release at lower pH [42].

In case of Curcumin, it was observed that less than 20% of the loaded drug was released at pH 5 and 40 °C, but more than 80% release was observed at pH 7.4 and 40 °C **(figure 2.4)**. As stated

above, the curcumin is expected to get entrapped into CD cavity as well as polymer matrix. Hence, drug release behavior is attributed to both the diffusion effect (explained in case of DOX) as well as the host guest interaction in CD cavity [43]. The pH response of curcumin release shows reverse trend as that of DOX release. This is due to the fact that curcumin is hydrophobic in nature, and is not expected to form electrostatic interactions with polymer chains. Moreover, with the increase in external pH, swelling of anionic polymer increases due to increased ionic strength of external media. This is attributed to presence of insoluble COOH groups that get ionized to COO- ions at pH above 4.5. The presence of such large number of anionic groups on the polymer leads to repulsion amongst the polymer chains and thus increased swelling of the polymer [44]. This phenomenon is enhanced at pH 7.4. Thus at pH 5.0 the drug release occurs only due to release of drug from the cavity of cyclodextrin and a slow release from polymeric matrix, whereas at pH 7.4 the enhanced release from the polymer matrix results in a higher drug release from the nanoconjugates.

It is important to note that CD plays an influential role in boosting drug payload as well as rate of release in case of hydrophobic drugs. The encapsulation in CD cavity occurs when hydrophobic drug molecules displace enthalpy rich water molecules that are initially present in the cavity. This creates an apolar-apolar association and thus causes a decrease in the ring strain of CD [45]. The release of drug does not involve any formation or breaking of covalent bonds on the contrary it is associated with the increase of a large number of water molecules in the surrounding environment that has the ability to again displace the drug molecules from the cavity [46].

Furthermore, in case of both DOX and curcumin, higher rate of drug release is observed at elevated temperature due to thermoresponsive characteristic of PNIPAM. Below the LCST (40°C for NIPAM) the polymer has the ability to form hydrogen bonds with surrounding water molecules which leads to hydration [47]. When the temperature is raised above LCST, the water molecules are forced out of the polymer structure into the bulk as it is more favorable. This results in the partial degradation and agglomeration of the polymer chains which also results in conformational changes, called coil to globule transformations. Such conformational changes lead to sudden diffusion of entrapped drug molecules, resulting into higher rate of drug release.

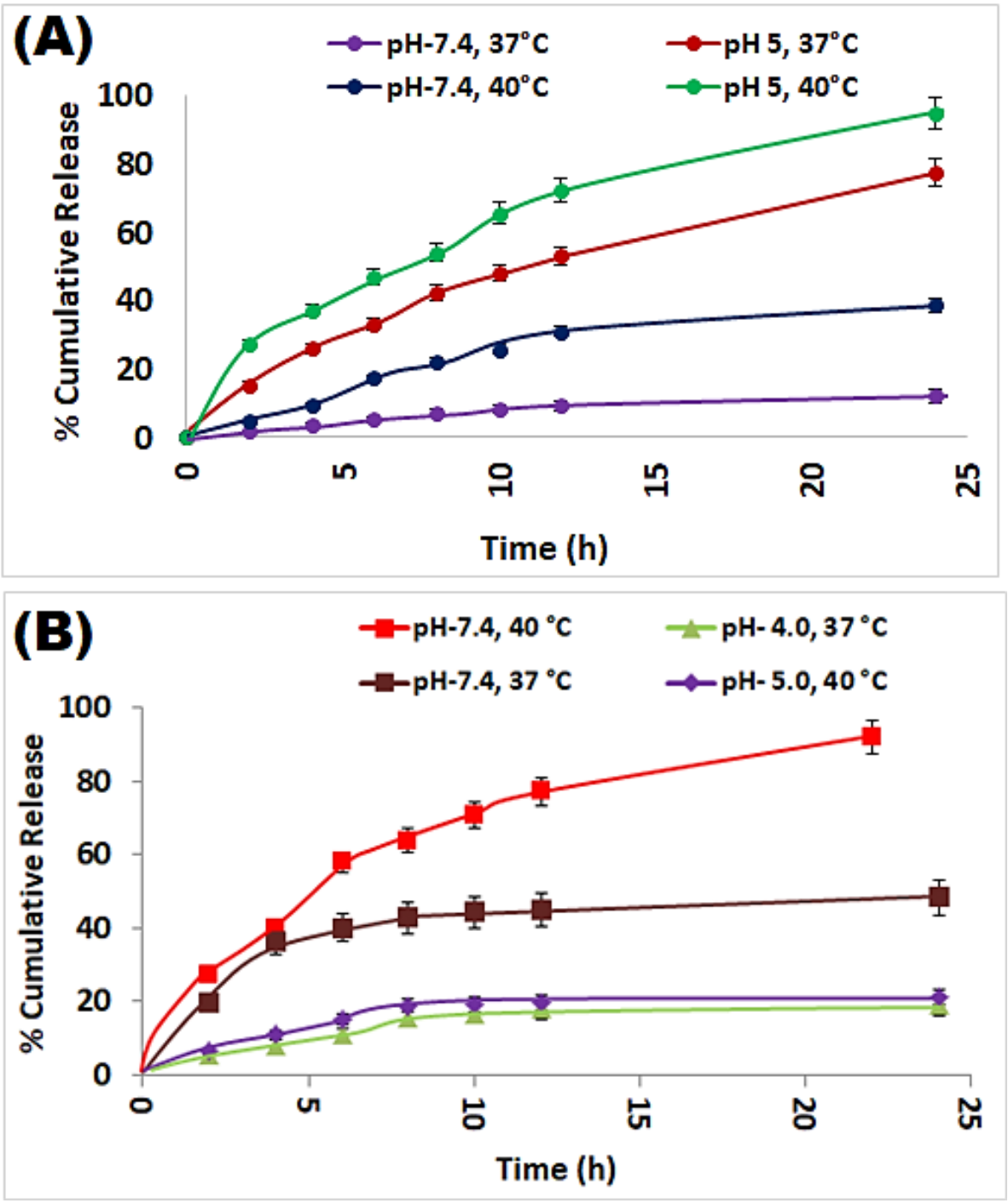


**Figure 2.4: Percentage cumulative release profile for (A) DOX and (B) Curcumin under various physiological conditions**

### 2.3.5 Mathematical modelling of the drug release profiles

The drug release kinetics and mechanism was determined by fitting the data in various kinetics models as described below (Figure S7-S14) [48,19,49].

$$\text{Zero order: } Qt/Q_0 = K_0t$$

$$\text{First order: } \text{In } Qt/Q_0 = K_1t$$

$$\text{Higuchi's model: } Q = K_H\, t^{1/2}$$

The values of co-relation coefficient ($R^2$) for Higuchi order release were highest as compared to other models for both DOX as well as curcumin **(Figures 2.5 to 2.12; Table 2.1 and 2.2)**. It can be said that the release of the drugs from the nanoconjugates follow Higuchi order kinetics. Further, to determine whether the diffusion from the polymeric scaffold was Fickian or non-Fickian, Korsmeyer-Peppas model was employed [50].

$$\log(M_t/M_\infty) = n \log t + \log k_p$$

Mt and $M_\infty$ corresponds to cumulative amount of released drug at time t and infinite time, respectively, *k* is Korsmeyer release constant and *n* is the diffusional exponent. The values of n for the Korsmeyer kinetics model at all the pH values were above 0.5 hence; it signifies that drug release from the nanoconjugates exhibit non-Fickian diffusion [51].

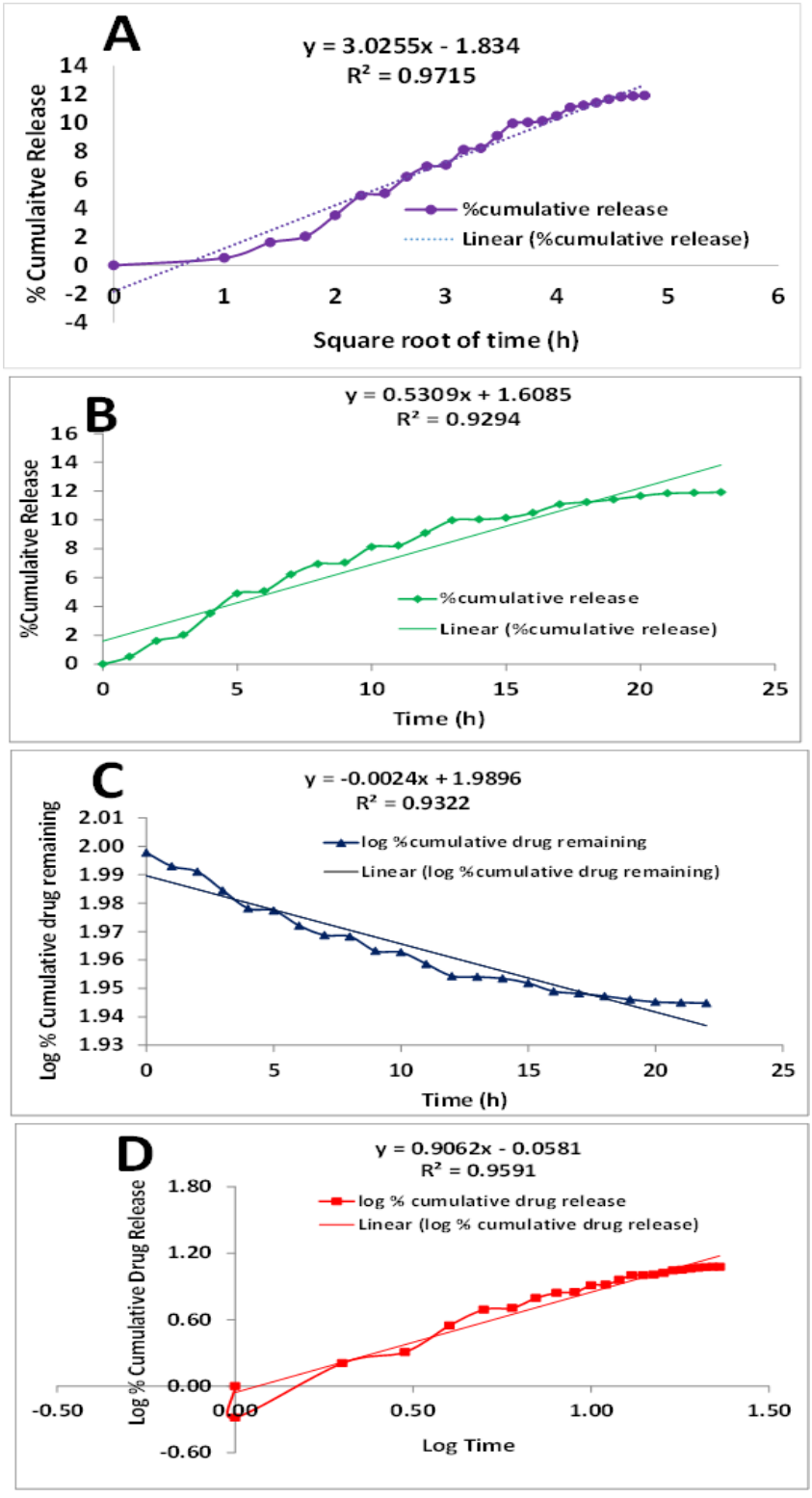


**Figure 2.5: Release kinetics of DOX from nanoconjugates at pH-7.4, 37°C (A) Higuchi model (B) Zero order, (C) First Order and (D) Korsmeyer-Peppas model**

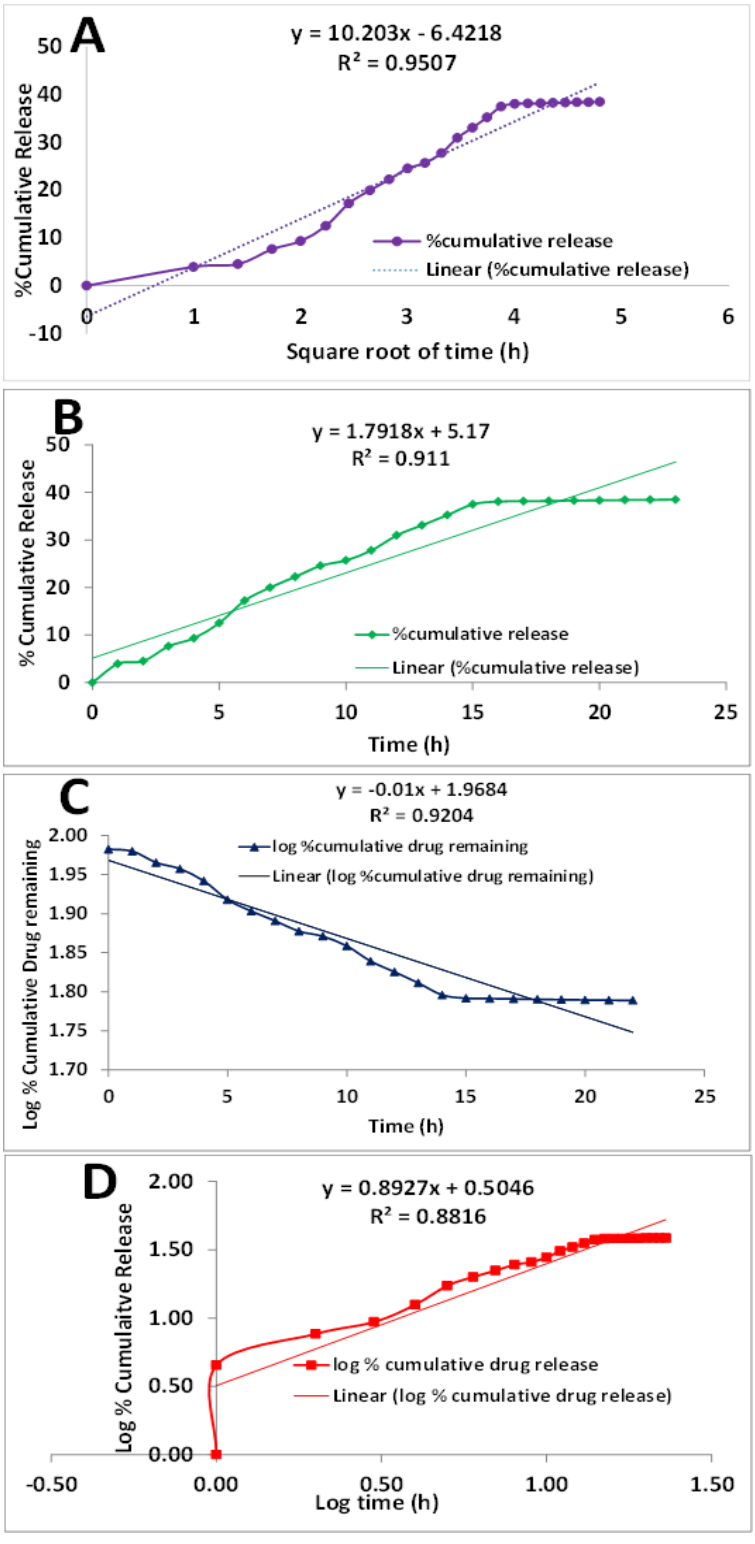


**Figure 2.6: Release kinetics of DOX from nanoconjugates at pH-7.4, 40°C (A) Higuchi model (B) Zero order,(C) First Order and (D) Korsmeyer-Peppas model**

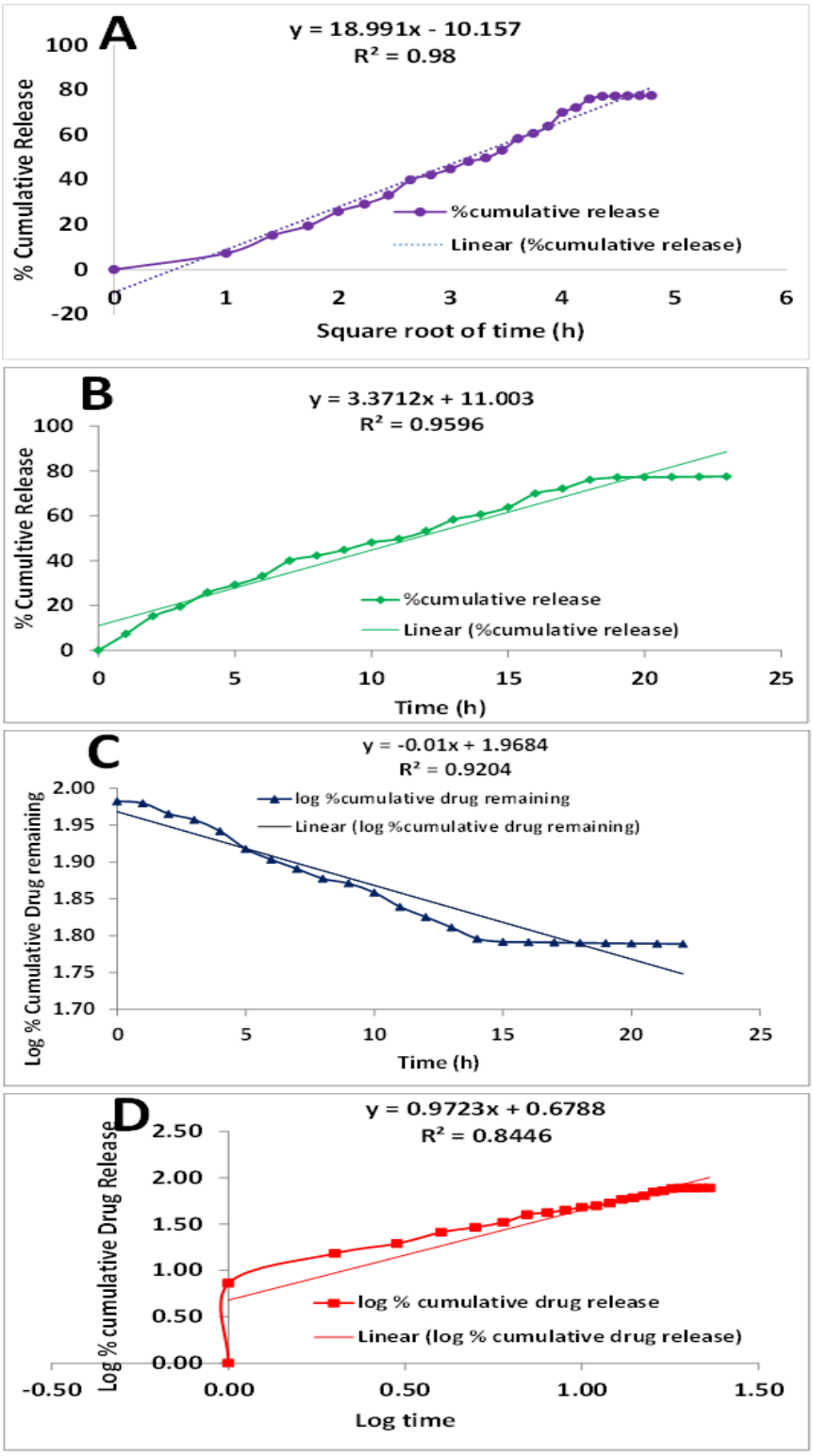


**Figure 2.7: Release kinetics of DOX from nanoconjugates at pH-5.0, 37°C (A) Higuchi model (B) Zero order,(C) First Order and (D) Korsmeyer-Peppas model**

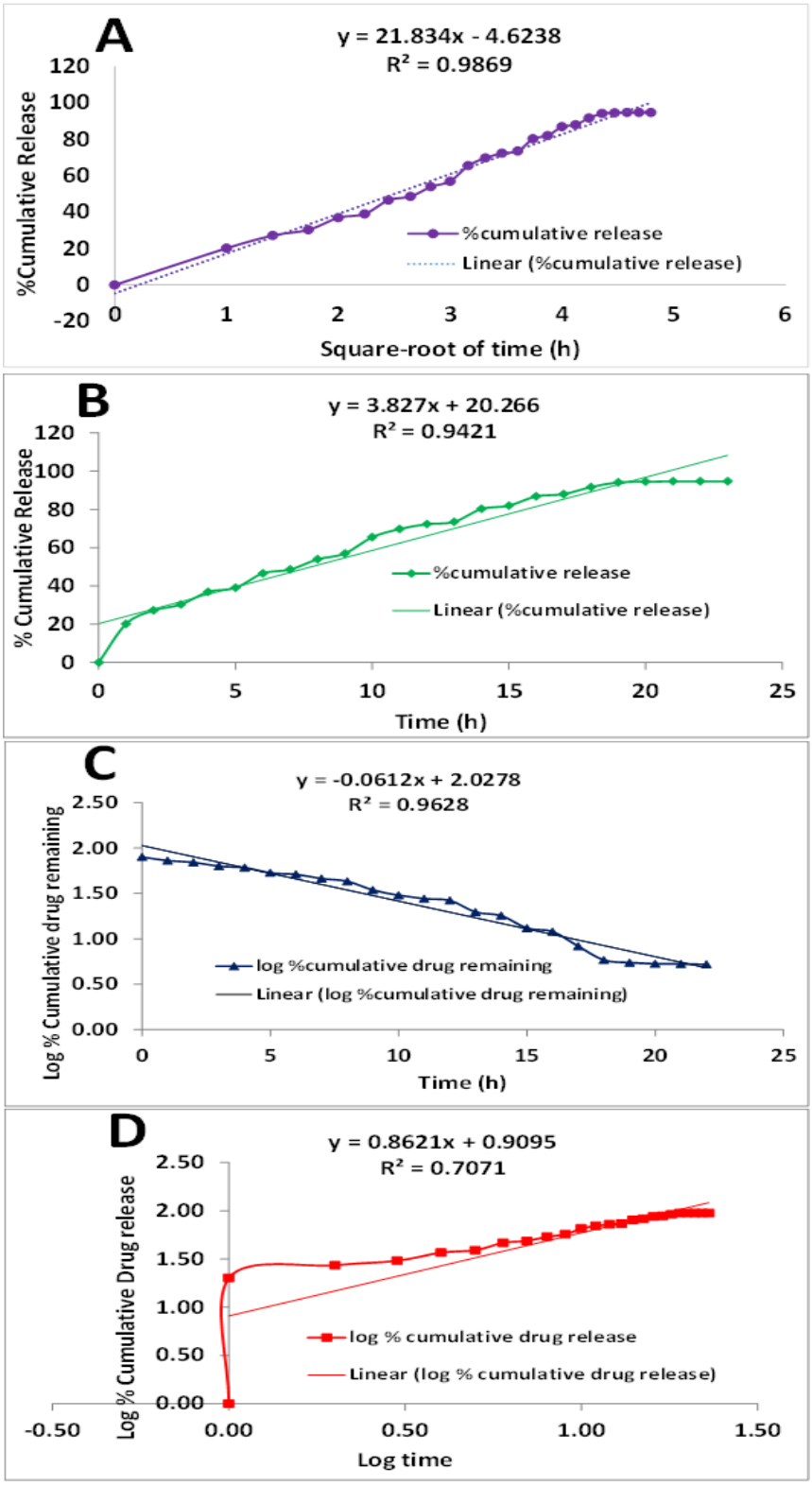


**Figure 2.8: Release kinetics of DOX from Nanoconjugates at pH-5.0, 40°C (A) Higuchi model (B) Zero order,(C) First Order and (D) Korsmeyer-Peppas model**

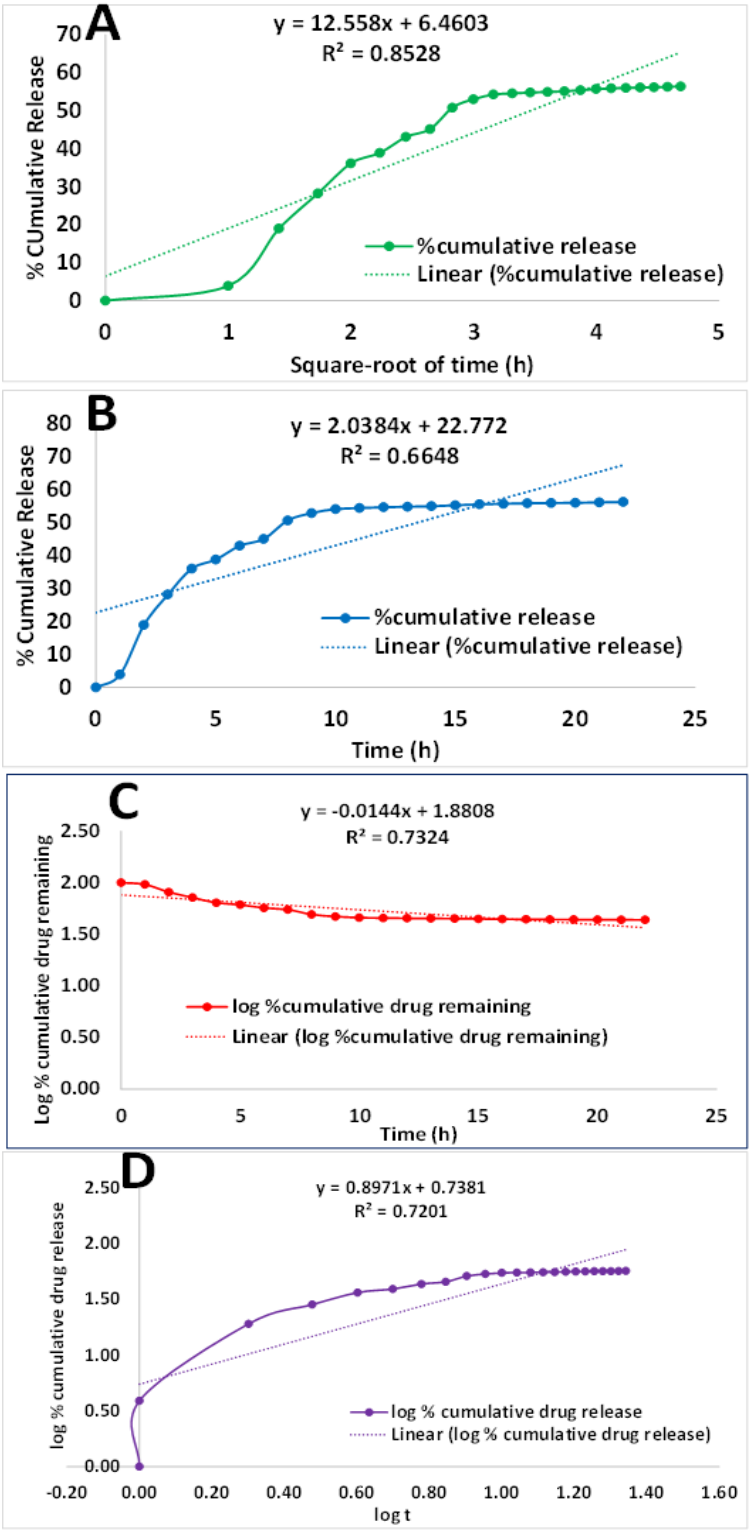


**Figure 2.9: Release kinetics of Curcumin from Nanoconjugates at pH-7.4, 37°C (A) Higuchi model (B) Zero order, (C) First Order and (D) Korsmeyer-Peppas model**

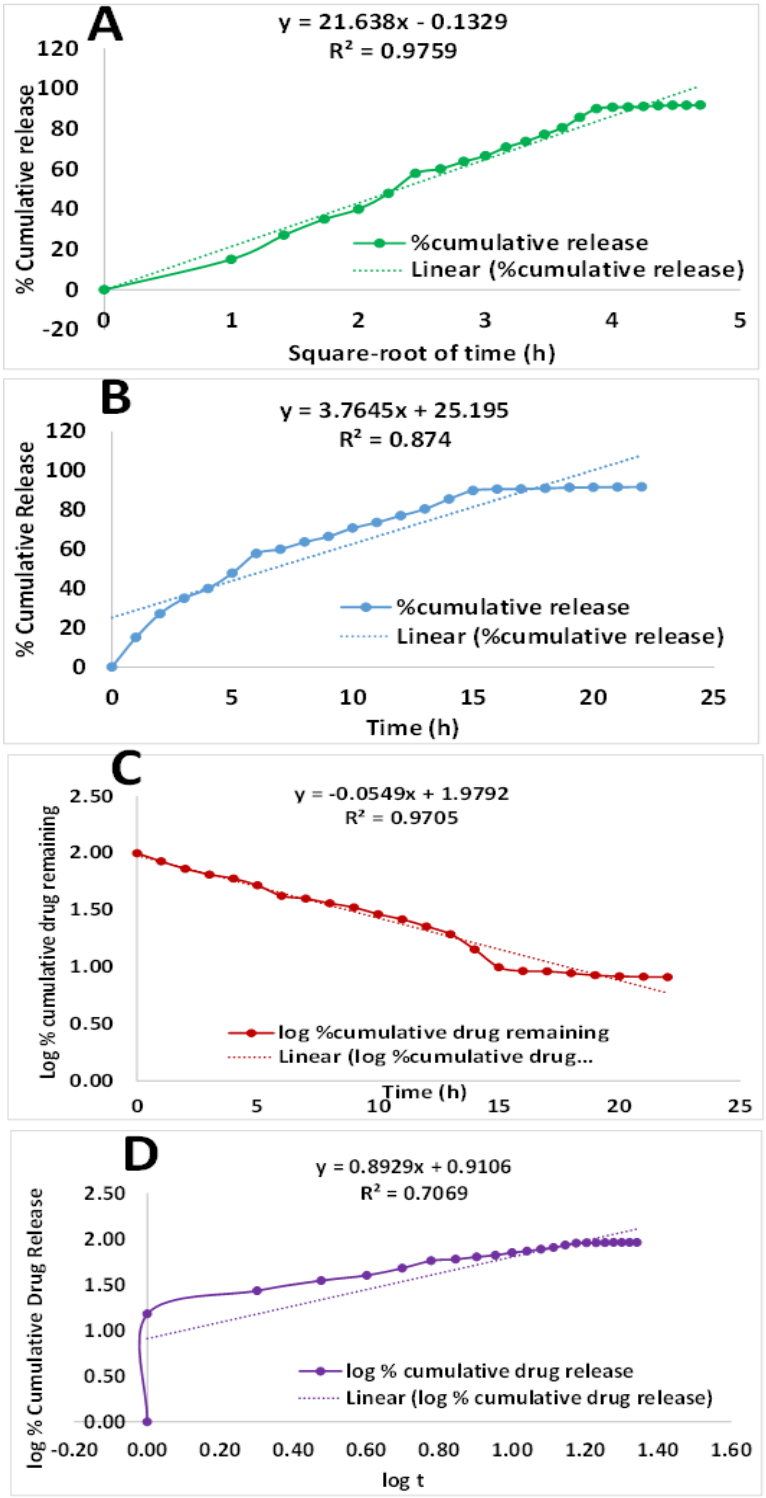


**Figure 2.10: Release kinetics of Curcumin from Nanoconjugates at pH-7.4, 40°C (A) Higuchi model (B) Zero order,(C) First Order and (D) Korsmeyer-Peppas model**

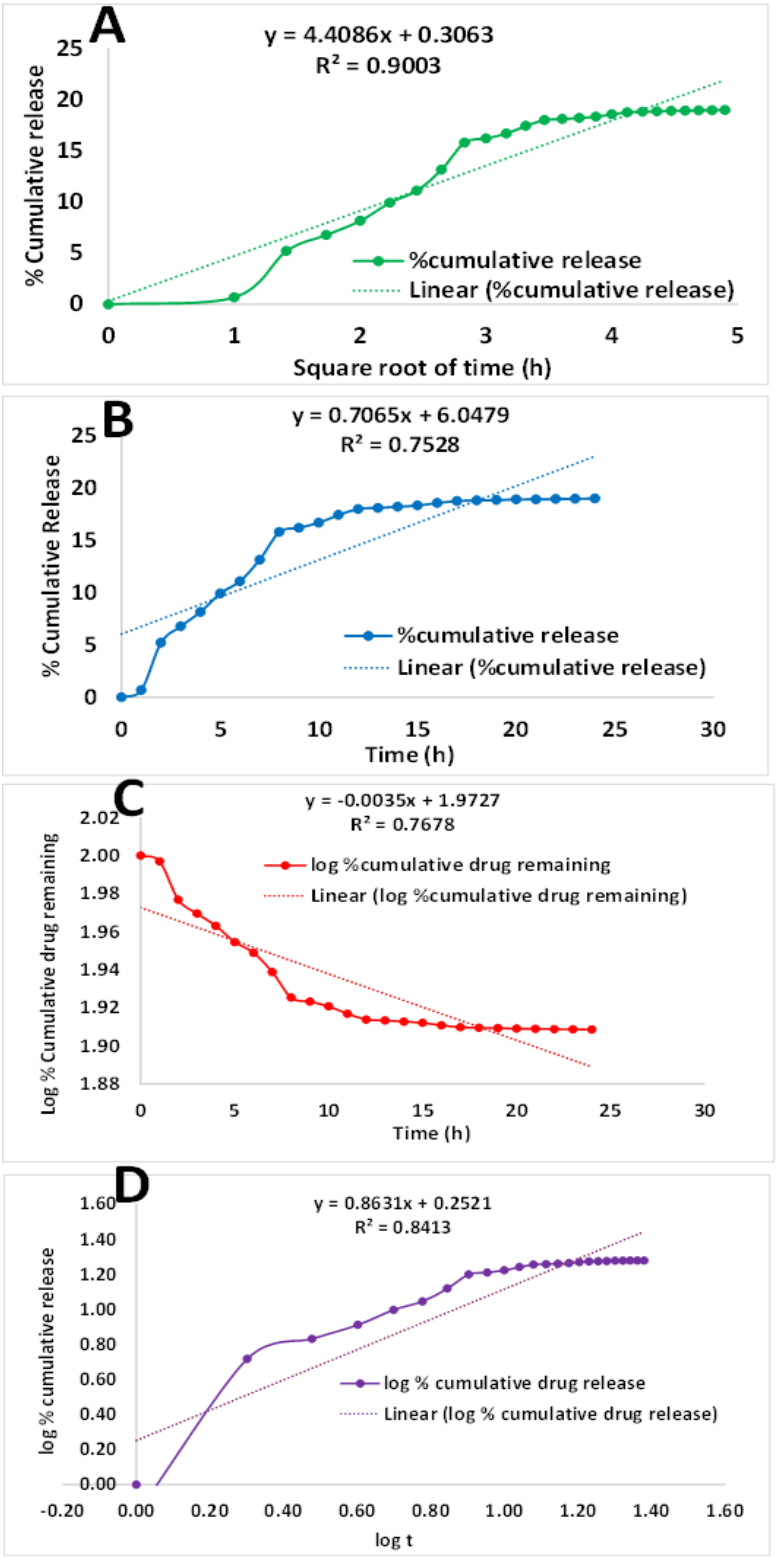


**Figure 2.11: Release kinetics of Curcumin from Nanoconjugates at pH-5.0, 37°C (A) Higuchi model (B) Zero order,(C) First Order and (D) Korsmeyer-Peppas model**

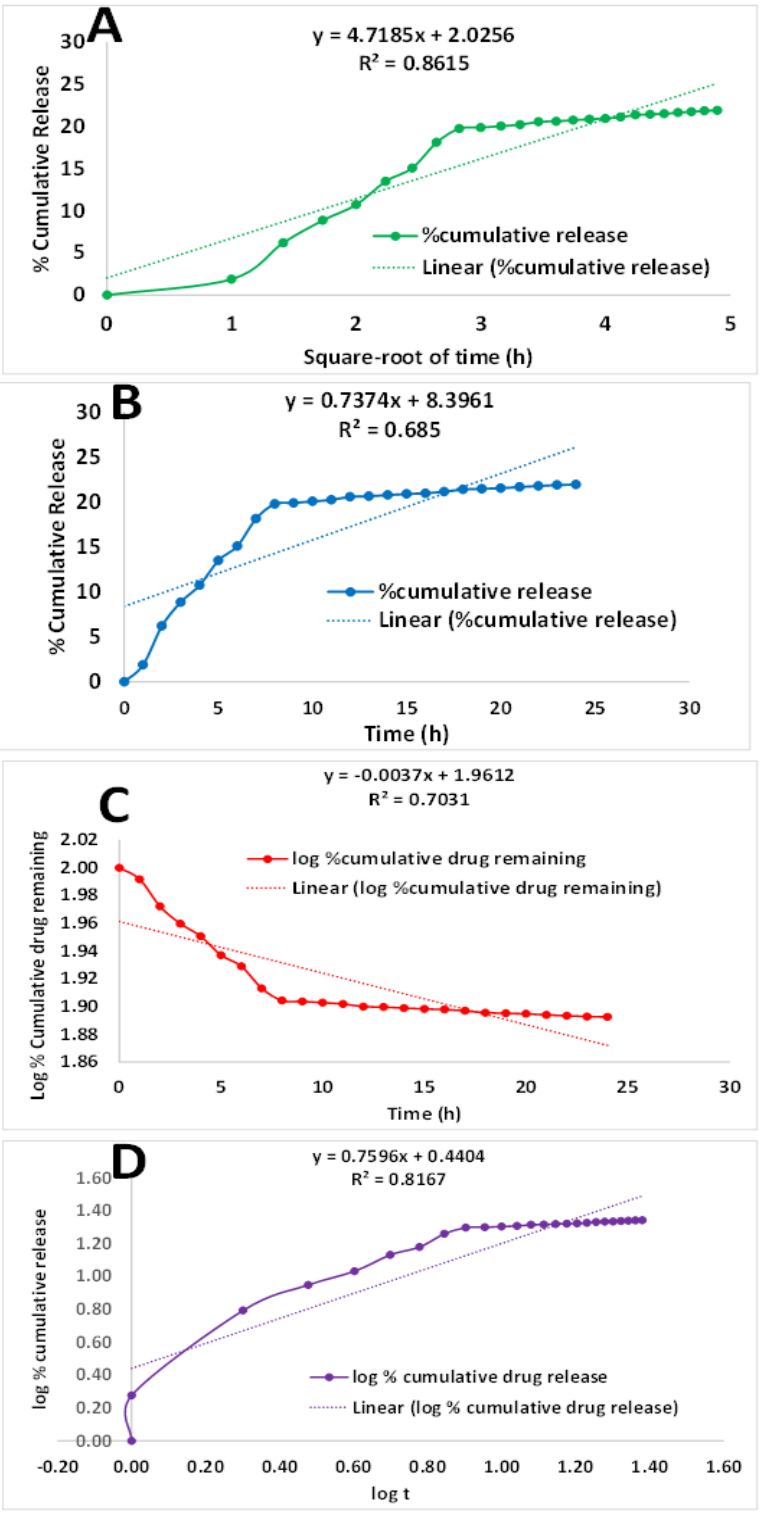


**Figure 2.12: Release kinetics of Curcumin from Nanoconjugates at pH-7.0, 37°C (A) Higuchi model (B) Zero order,(C) First Order and (D) Korsmeyer-Peppas model**

**Table 2.1: Mathematical modelling data for DOX release from nanoconjugates**

| Temperature (°C) | Kinetic Model | Correlation Coefficient ($R^2$) |
|---|---|---|
| **37 °C (pH 7.4)** | Higuchi order | 0.9715 |
| | Zero Order | 0.9294 |
| | First Order | 0.9322 |
| | Korsmeyer-Peppas order | 0.9591 |
| **37 °C (pH 5.0)** | Higuchi order | 0.9800 |
| | Zero Order | 0.996 |
| | First Order | 0.9795 |
| | Korsmeyer-Peppas order | 0.8446 |
| **40 °C (pH 7.4)** | Higuchi order | 0.9507 |
| | Zero Order | 0.9110 |
| | First Order | 0.9204 |
| | Korsmeyer-Peppas order | 0.8816 |
| **40 °C (pH 5.0)** | Higuchi order | 0.9869 |
| | Zero Order | 0.9421 |
| | First Order | 0.9628 |
| | Korsmeyer-Peppas order | 0.7071 |

**Table 2.2: Mathematical modelling data for curcumin release from nanoconjugates**

| Temperature (°C) | Kinetic Model | Correlation Coefficient ($R^2$) |
|---|---|---|
| **37 °C (pH 7.4)** | Higuchi order | 0.8528 |
| | Zero Order | 0.6648 |
| | First Order | 0.7324 |
| | Korsmeyer-Peppas order | 0.7201 |
| **37 °C (pH 5.0)** | Higuchi order | 0.9003 |
| | Zero Order | 0.7528 |
| | First Order | 0.7678 |
| | Korsmeyer-Peppas order | 0.8413 |
| **40 °C (pH 7.4)** | Higuchi order | 0.9759 |
| | Zero Order | 0.8740 |
| | First Order | 0.9705 |
| | Korsmeyer-Peppas order | 0.7069 |
| **40 °C (pH 5.0)** | Higuchi order | 0.8615 |
| | Zero Order | 0.6850 |
| | First Order | 0.7031 |
| | Korsmeyer-Peppas order | 0.8167 |

### 2.3.6 Cell Viability Assay

The cytotoxic properties were determined by quantifying the cell viability using MTT (a tetrazolium dye) assay. In this assay, the dye MTT is subjected to reduction by the mitochondrial enzymes thus forming a blue colored compound [52]. The intensity of this dye holds proportionality to the number of viable cells which is determined by colorimetric estimation. The nanoconjugates with and without drug, were screened for MTT assay using cervical cancer cell line (Hela) and the results are shown in **Figure 2.13 and 2. 14**.

.

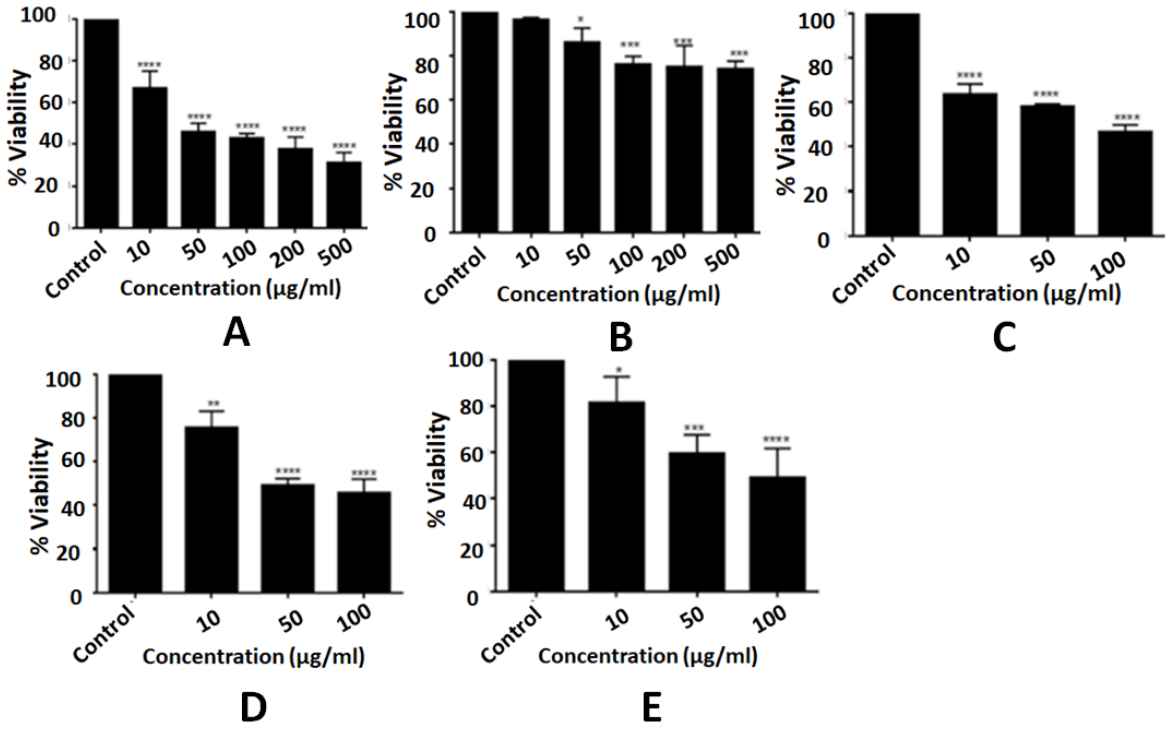


**Figure 2.13: Study of Cell viability on Hela cells. (A)Curcumin (B) Nanoconjugates (C) Curcumin loaded nanoconjugates (D) Curcumin loaded nanoconjugates in presence of magnet (E) Curcumin loaded nanoconjugates after 12 hours of dosing. Cells were incubated with different concentration of drug-loaded nanoconjugates for 24/12 hours. Cell Viability was calculated by MTT Assay. % Viability= (Absorbance of Test well) / (Absorbance of control well)*100 plotted against the concentration of drug loaded nanoconjugates.**

The treatment with model drugs accounted for significant decrement in cell viability at all the doses (10, 50, 100, 200 and 500 µg/ml) studied herein. The nanoconjugates accounted for >74% cell viability at a dose range (10 to 500 µg/ml) indicating its non-toxicity. However, drug loaded nanoconjugates accounted for significant decrement in cell viability at 10 and 50 µg/ml. It is interesting to note that a further decrement in cell viability was recorded in presence of magnet. It was observed that cytotoxicity of curcumin was enhanced when nanoconjugates serve as drug carriers. This can be attributed to the efficiency of the nanoconjugates in transporting larger amounts of drugs into the cell via endocytosis rather than its transport through ion channels [53].

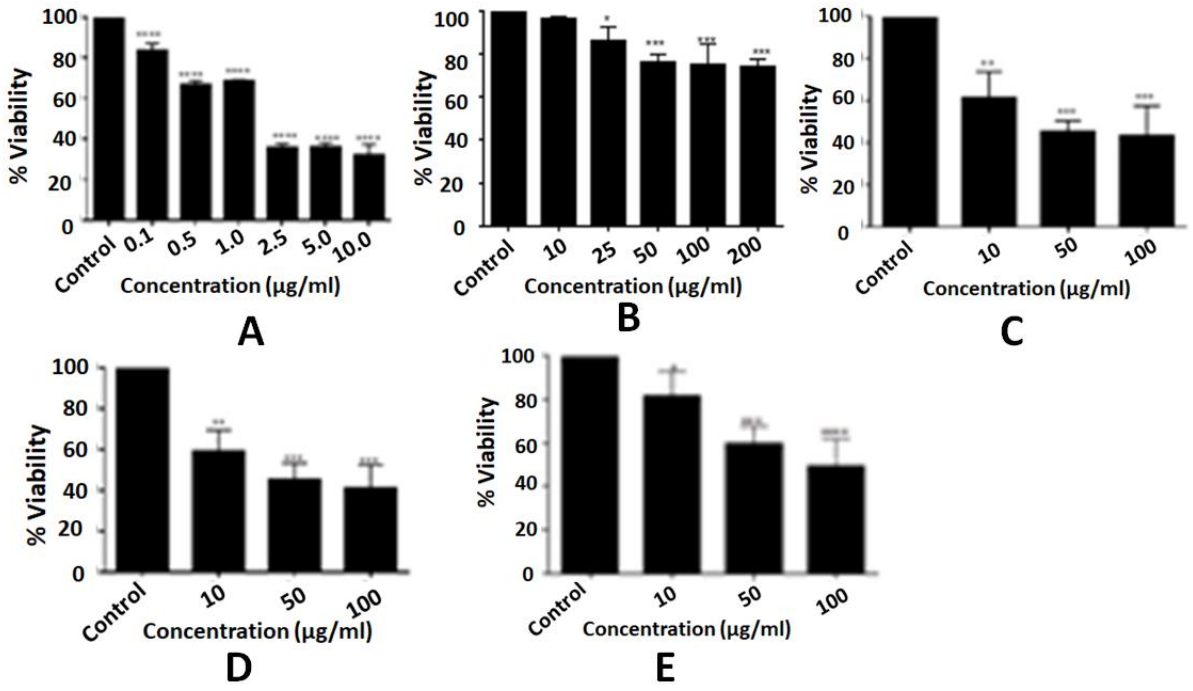


**Figure 2.14: Study of Cell viability on Hela cells. (A)DOX (B) Nanoconjugates (C) DOX loaded nanoconjugates (D) DOX loaded nanoconjugates in presence of magnet (E) DOX loaded nanoconjugates after 12 hours of dosing.**

A decrease in cell viability may be because curcumin after endocytosis accumulates in the endoplasmic reticulum (ER) membrane, which causes a reduction in the intracellular iron pool. This causes an elongation in the G1 phase of the cell cycle resulting in a retarded cell growth in vitro [43].

### 2.3.7 Hemolysis Assay

Intravenous administration of therapeutant or a nanoconjugate brings in contact with blood cells and therefore assessing its hemolytic property is of vital importance. The nanoconjugates with therapeutic potential may show promising results in in-vitro experiments but may induce hemolysis [54].

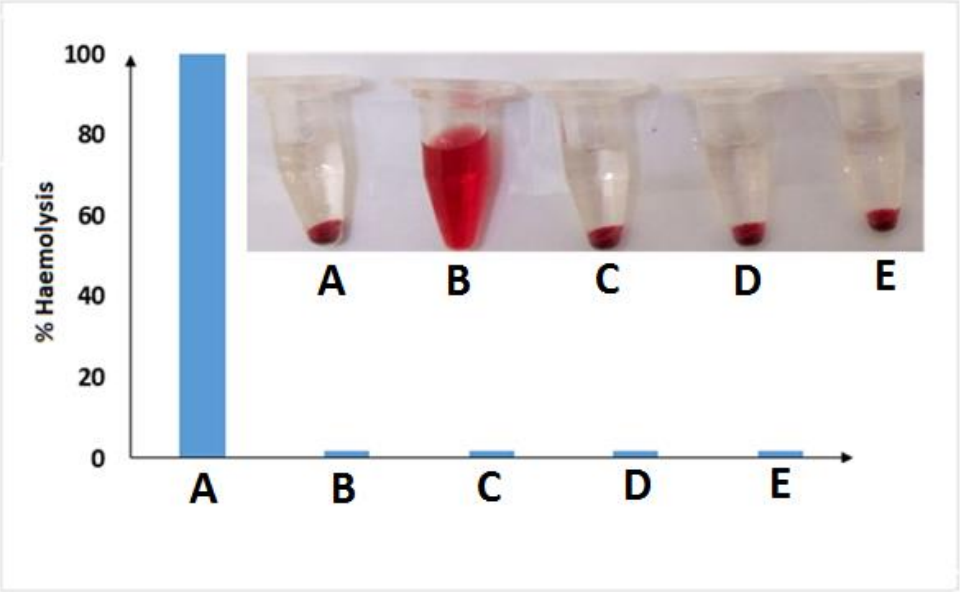


**Figure 2.15: Hemolysis assay of nanoconjugates where, (A) Positive Control (B) Negative Control (C) Curcumin (D) Nanoconjugates (E) Curcumin loaded Nanoconjugates**

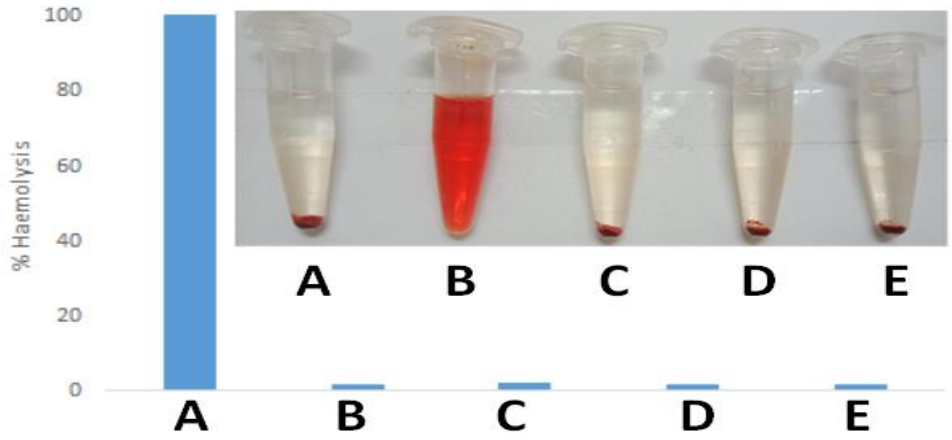


**Figure 2.16: Hemolysis assay of nanoconjugates where, (A) Positive Control (B) Negative Control (C) DOX (D) nanoconjugates (E) DOX loaded Multifunctional Nanoconjugates.**

In the present study hemolysis assay was used to establish hemocompatibility of drug and nanoconjugates with an aim to analyze the effect on erythrocyte membrane and possibility of hemolysis. Curcumin showed 1.6 % hemolysis whereas nanoconjugates, DOX and curcumin loaded nanoconjugates both exhibit 1.7 % hemolysis upon incubation.

Thus it can be concluded from the results that Curcumin, nanoconjugates and Curcumin loaded nanoconjugates did not induce hemolysis **(Figure 2.15 and 2.16)** and hence can be considered as hemocompatible.

### 2.3.8 Internalization test

The nanoconjugates shows auto-fluorescence in green filter (Ex/Em: 485-520 nm). Data showcased herein shows HeLa cells showing prominent fluorescence after treatment with nanoconjugates. A comparison with nanoconjugates free of folic acid shows that folate conjugation significantly enhances the internalization. In order to understand the effect of magnetic field this experiment was also carried out in presence of magnet. Results reveal that presence of magnet accounted for moderately higher internalization of nanoconjugates as evidenced by photographs **(figure 2.17)**. These results also confirm the ability of nanoconjugates to cross plasma membrane and get internalized in the cytosol of HeLa cells. Healthy cellular morphology observed herein corroborates the findings of cell viability assay.

### 2.3.9 Cell mortality test

Cell mortality test was performed using propidium iodide staining that is known to penetrate necrotic or dead cells whereas, live cells remain unstained. In our study, the control cells did not show any fluorescence indicating at their viable condition **(figure 2.18A & C)**.

However, Curcumin and DOX treatment accounted for moderate cell mortality as seen in form of PI positive cells. Drug loaded nanoconjugates accounted for a prominent response in form of more cells showing PI positive staining **(figure 18 B, C, D & F)**. These results provide important qualitative evidence on nanoconjugates mediated increased uptake of drugs that accounts for visibly higher cell mortality.

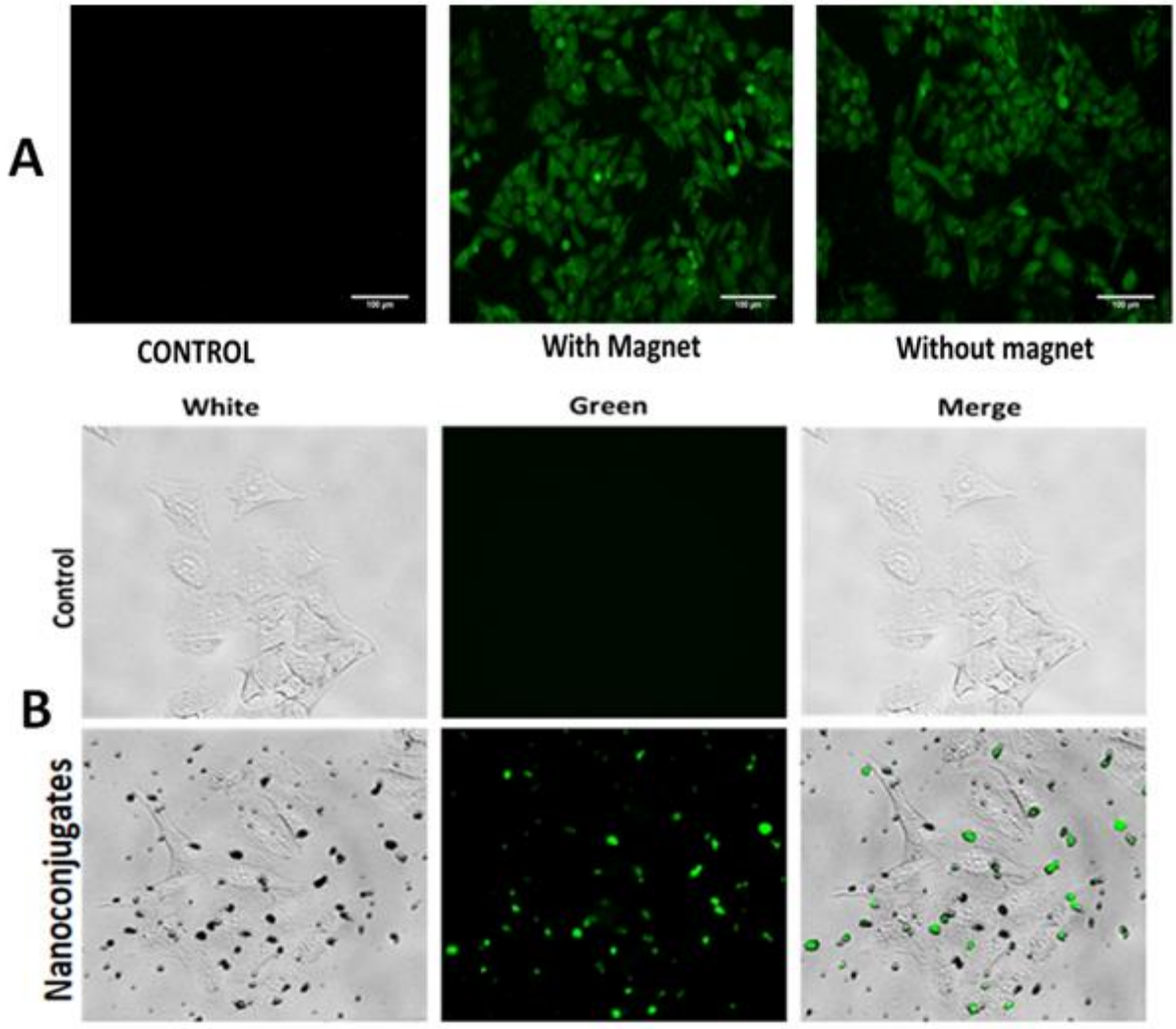


**Figure 2.17: Internalization of nanoconjugates on Hela cells (A) In presence of nanoconjugates conjugated with folic acid (with and without magnet) (B) In presence of nanoconjugates without folic acid conjugation.**

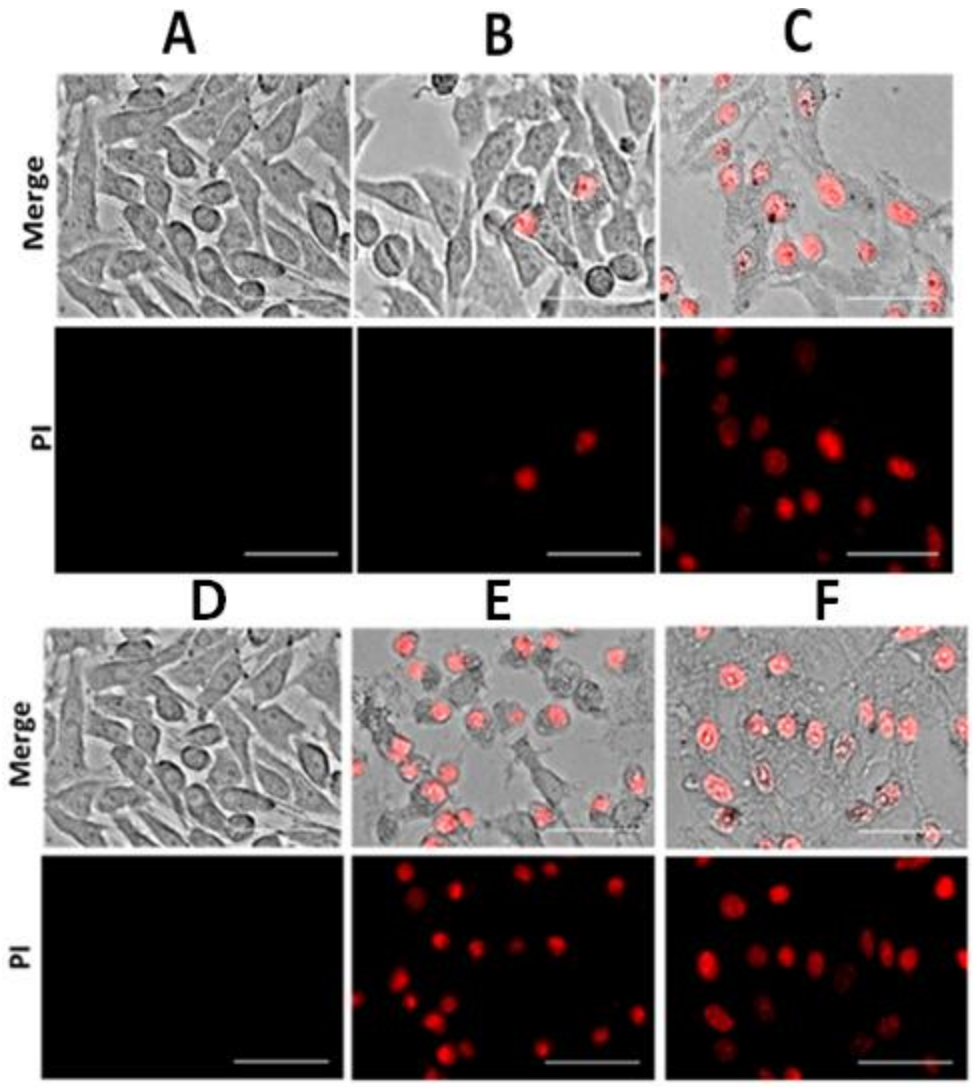


**Figure 2.18: PI staining of Hela cells. Cells undergoing necrosis were stained by PI. Here, (A) Control (B) Curcumin (C) Curcumin loaded nanoconjugates (D) Control (E) DOX (F) DOX loaded nanoconjugates (Scale bar= 50 µm.)**

### 2.3.10 In-Vivo Studies

Hepatocellular carcinoma (HCC) is a one of the predominant cause of cancer deaths worldwide, in patients suffering from chronic liver disease and cirrhosis. In our study, experimentally induced tumor in rodent model were treated with DOX alone or DOX-loaded nanoconjugates. Results reveal that the body weight of animals and whole weight of liver showed significant increase that is attributable to corresponding tumor growth in liver **(figure 2.19 A & B)**.

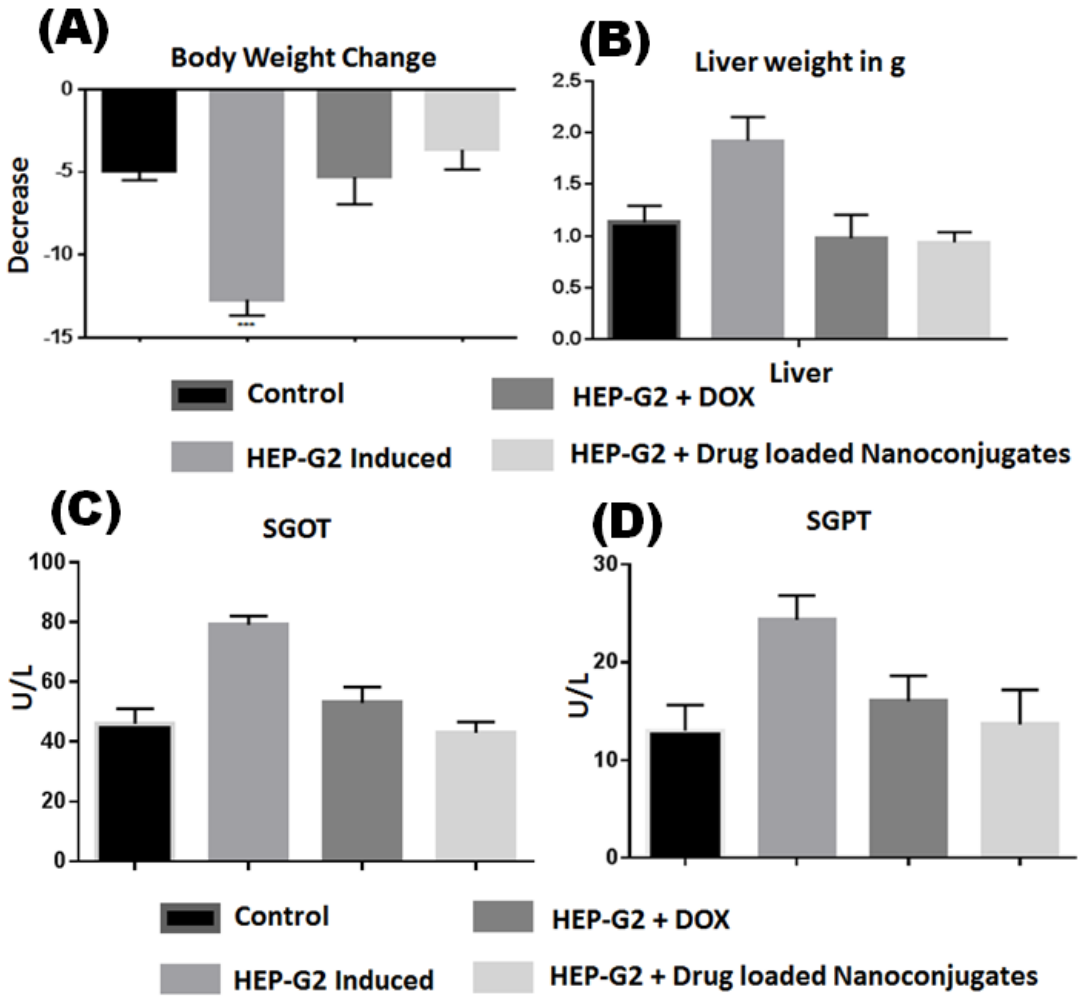


**Figure 2.19: Changes in the (A) Body weight of animals and (B) Weight of liver, measurements of liver indices (C) SGOT and (D) SGPT**

However, DOX or DOX loaded Nanoconjugates treated groups did not record such an increase and the observed values were comparable to that of control. The liver function test (Serum SGPT and SGOT levels **(figure 2.19 C & D)** showed a significant increment in HCC group. But the same showed significant decrement in activity levels in DOX and DOX loaded Nanoconjugates treated groups. This suggests that the functional indices of liver were restored to near normal levels.

Matrix metallopeptidase (MMP) 2 and 9 are indicated for their role in extracellular matrix modulation, remodeling and angiogenesis. Especially role of MMP-9 has been emphasized in

tumor progression invasion and metastasis [55]. In our study, HCC group recorded significantly elevated plasma levels of MMP-2 and 9 confirming onset and progression of hepatic tumor. The decrease in the levels of both these biomarkers post treatment with drug loaded nanoconjugates are an indication of effective treatment **(figure 2.20 A & B)**.

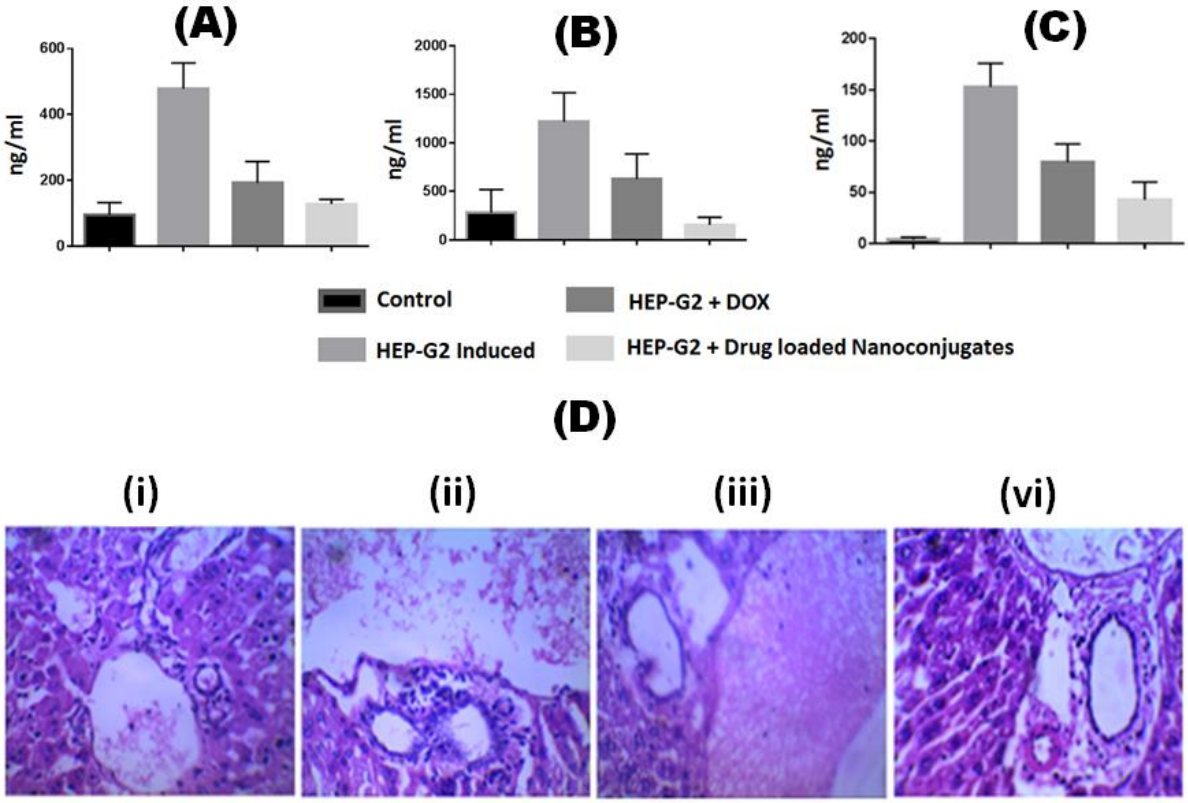


**Figure 2.20: Quantification of the biomarkers levels specific to cancer as observed in animals (A) MMP-2, (B) MMP-9 and (C) AFP. (D) Liver Sections of (i) Control and animals dosed with (ii) HEP-G2 (iii) DOX and (iv) DOX loaded nanoconjugates at 40X magnification.**

Circulating levels of Alpha Fetoproteins (AFP) are commonly assessed to monitor presence and progression of HCC [56] . Hence, AFP is an important biomarker of HCC and was found to be significantly elevated in the HCC induced group. Significantly lowered levels of AFP following DOX treatment validates efficacy of the drug as per published report [57]. It is interesting to note that DOX loaded nanoconjugates recorded lower AFP values than DOX treated groups suggesting that nanoconjugates are instrumental in targeted drug delivery **(figure 20 C).**

Histoarchitechture of liver by H&E staining showed distorted liver lobes, de-arrangement of hepatic cod and canaliculi. This supports previous observations in HCC groups. DOX treatment accounted for significant decrement in MMP-2 and 9 levels that were supported by microscopic observations of lesser extent of cellular de-arrangement in liver **(figure 20 D)**. Liver sections of DOX loaded nanoconjugates group were similar to control and the plasma levels of MMP-2 and 9 were comparable to control. These observations are of relevance that confirms DOX induced prevention of tumor progression that is further enhanced by use of nanoconjugates (figure 9). Overall, in-vivo studies provide valuable insight on efficient delivery of DOX to HCC tissue by nanoconjugates. Biomarkers of liver function, tumor progression, matrix modulation and inflammation provide compelling positive evidences in this regard.

### 2.4 Conclusion

The results manifest the potential of synthesized β-cyclodextrin based nanoconjugates as smart theranostic agents possessing multiple properties like fluorescence imaging, cancer cell-targeting, dual stimuli response and dual drug delivery. All the conjugated functionalities were successfully found to exhibit their properties individually within the single nano-system.

The nanoconjugates could competently load and release hydrophilic as well as hydrophobic drug, owing to the presence of cyclodextrin. On application of external magnetic field the material could quickly reach the therapeutic temperature required for destruction of cancer cells and therefore can be used effectively for hyperthermia therapy. The magnetic manipulation of the nanoconjugates resulted in a moderately increased internalization in-vitro. Fluorescent imaging of the nanoconjugates within the cells demonstrated an increased internalization due to folic acid conjugation. In particular, the nanoconjugates were found to effectively enhance the endocytosis of anticancer curcumin that is poorly bioavailable. The in vivo studies corroborate with the in-vitro data showing a significant tumor regression when drug loaded nanoconjugates were injected into the animals. Thus the synthesized nanoconjugates with a synergistic combination of multiple functionalities were observed have potent application to act as effective theranostic agents in the field of cancer therapy.

**2.5 References**


1. Ang CY, Zhao Y, Tan SY. *Org Biomol Chem*. 2014; 12: 4776–4806.
2. Cohen K, Emmanuel R, Kisin-finfer E, Shabat D, Peer D. *ACS Nano*. 2014; 8: 2183–2195.
3. Shen S, Liu M, Li T, Lin S, Mo R. *Biomater Sci*. 2017; 5: 1367-.
4. Lu N, Tian Y, Tian W, Huang P, Liu Y, Tang Y, Wang C, Wang S, Su Y, Zhang Y, Pan J, Teng Z, Lu G. *ACS Appl Mater Interfaces*. 2016; 8: 2985–2993.
5. Wang H, Ke F, Mararenko A, Wei Z, Banerjee P, Zhou S. *Nanoscale*. 2014; 6: 7443–7452.
6. Nan X, Zhang X, Liu Y, Zhou M, Chen X, Zhang X. *ACS Appl Mater Interfaces*. 2017; 9: 9986–9995.
7. Liu B, Zhang X, Li C, He F, Chen Y, Huang S, Jin D, Yang P, Cheng Z, Lin J. *Nanoscale*. 2016; 8: 12560–12569.
8. Chen P, Song H, Yao S, Tu X, Su M, Zhou L. *RSC Adv*. 2017: 29025–29034.
9. Hu Q Da, Tang GP, Chu PK. *Acc Chem Res*. 2014; 47: 2017–2025.
10. Kumar D, Krishnan Y, Paranjothy M, Pal S. *J Phys Chem B*. 2017; 121: 2864–2872.
11. Eid EEM, Abdul AB, Suliman FEO, Sukari MA, Rasedee A, Fatah SS. *Carbohydr Polym*. 2011; 83: 1707–1714.
12. Solanki AR, Kamath B V., Thakore S. *J Appl Polym Sci*. 2015; 132: 1–12.
13. Solanki A, Sanghvi S, Devkar R, Thakore S. *RSC Adv*. 2016; 6: 98693–98707.
14. Solanki A, Mehta J, Thakore S. *Carbohydr Polym*. 2014; 110: 338–344.
15. Solanki A, Das M, Thakore S. *Carbohydr Polym*. 2018; 181: 1003–1016.
16. Luisa M, Emma MR, Botto C, Augello G, Azzolina A, Gaudio F Di, Craparo EF, Cavallaro G, Bachvarov D. *J Agric Food Chem*. 2017; 65: 1342–1352.
17. Badruddoza AZM, Rahman MT, Ghosh S, Hossain MZ, Shi J, Hidajat K, Uddin MS. *Carbohydr Polym*. 2013; 95: 449–457.
18. Pradhan P, Giri J, Rieken F, Koch C, Mykhaylyk O, Döblinger M, Banerjee R, Bahadur D, Plank C. *J Control Release*. 2010; 142: 108–121.
19. Kashyap S, Singh N, Surnar B, Jayakannan M. *Biomacromolecules*. 2015.
20. Evans BC, Nelson CE, Yu SS, Beavers KR, Kim AJ, Li H, Nelson HM, Giorgio TD, Duvall CL. *J Vis Exp*. 2013: 7–11.

21. Sharma P, Rana S, Barick KC, Kumar C, Salunke HG, Hassan PA. *New J Chem*. 2014; 38: 5500–5508.
22. Cummings BS, Wills LP, Schnellmann RG. *Curr Protoc Phamacol*. 2004; 1: 1–30.
23. Can K, Ozmen M, Ersoz M. *Colloids Surfaces B Biointerfaces*. 2009; 71: 154–159.
24. Carmen Bautista M, Bomati-Miguel O, Del Puerto Morales M, Serna CJ, Veintemillas-Verdaguer S. *J Magn Magn Mater*. 2005; 293: 20–27.
25. Zhou, J.; Zhang X.; Dai, J.; Li J. *J Macromol Sci Part A Pure Appl Chem*. 2012; 49: 890–896.
26. Cesteros LC, Ramírez CA, Peciña A, Katime I. *J Appl Polym Sci*. 2006; 102: 1162–1166.
27. Gavira JM, Hernanz A, Bratu I. *Vib Spectrosc*. 2003; 32: 137–146.
28. Omer M, Haider S, Park S. *Polymer (Guildf)*. 2011; 52: 91–97.
29. Bafkary R, Khoee S. *RSC Adv*. 2016; 6: 82553–82565.
30. Park EJ, Draper DD, Flynn NT. *Langmuir*. 2007; 23: 7083–7089.
31. Togashi T, Naka T, Asahina S, Sato K, Takami S, Adschiri T. *Dalt Trans*. 2011; 40: 1073–1078.
32. Solanki A, Sanghvi S, Devkar R, Thakore S. *RSC Adv*. 2016; 6: 98693–98707.
33. Akbarzadeh A, Samiei M, Joo SW, Anzaby M, Hanifehpour Y, Nasrabadi HT, Davaran S. *J Nanobiotechnology*. 2012; 10: 1.
34. Badruddoza AZM, Rahman MT, Ghosh S, Hossain MZ, Shi J, Hidajat K, Uddin MS. *Carbohydr Polym*. 2013; 95: 449–457.
35. Deshpande NU, Jayakannan M. *Biomacromolecules*. 2017; 18: 113–126.
36. Coelho JF, Ferreira PC, Alves P, Cordeiro R, Fonseca AC, Góis JR, Gil MH. *EPMA J*. 2010; 1: 164–209.
37. Solanki A, Thakore S. *Int J Biol Macromol*. 2015; 80: 683–691.
38. Meier MM, Luiz MTB, Szpoganicz B, Soldi V. *Thermochim Acta*. 2001; 375.
39. Sharma P, Rana S, Barick KC, Kumar C, Salunke HG, Hassan PA. *New J Chem*. 2014; 38: 5500–5508.
40. Donadel K, Felisberto MD V, Fávere VT, Rigoni M, Batistela NJ, Laranjeira MCM. *Mater Sci Eng C*. 2008; 28: 509–514.
41. Zamora-Mora V, Fernández-Gutiérrez M, González-Gómez Á, Sanz B, Román JS, Goya GF, Hernández R, Mijangos C. *Carbohydr Polym*. 2017; 157: 361–370.

42. Zheng Y, Wang L, Lu L, Wang Q, Benicewicz BC. *ACS Omega*. 2017; 2: 3399–3405.
43. Minear S, Donnell AFO, Ballew A, Giaever G, Nislow C, Stearns T, Cyert MS. *Eukaryot Cell*. 2011; 10: 1574–1581.
44. Solanki A, Thakore S. *Int J Biol Macromol*. 2015; 80: 683–691.
45. Loftsson T, Brewster ME. *J Pharm Sci*. 1996; 85: 1017–1025.
46. Del Valle EMM. *Process Biochem.*, 2004, 39, 1033–1046.
47. Shiraga K, Naito H, Suzuki T, Kondo N, Ogawa Y. *J Phys Chem B*. 2015; 119: 5576–5587.
48. Jarosz M, Pawlik A, Szuwarzyński M, Jaskuła M, Sulka GD. *Colloids Surfaces B Biointerfaces*. 2016; 143: 447–454.
49. Tamayo A, Mazo MA, Veiga MD, Ruiz-caro R, Notario-pérez F, Rubio J. *Mater Sci Eng C*. 2017; 75: 1097–1105.
50. Dwivedi R, Singh AK, Dhillon A. *J Sci Adv Mater Devices*. 2017; 2: 45–50.
51. Lee PI. *J Control Release*. 1985; 2: 277–288.
52. Thounaojam MC, Jadeja RN, Valodkar M, Nagar PS, Devkar R V., Thakore S. *Food Chem Toxicol*. 2011; 49: 2990–2996.
53. Scarano W, Souza P De, Stenzel MH. *Biomater Sci*. 2014; 1.
54. Fischer D, Li Y, Ahlemeyer B, Krieglstein J, Kissel T. *Biomaterials*. 2003; 24: 1121–31.
55. Morini M, Mottolese M, Ferrari N, Ghiorzo F, Buglioni S, Mortarini R, Noonan DM, Natali PG, Albini A. *Int J Cancer*. 2000; 87: 336–342.
56. Nomura F, Ohnishi K, Tanabe Y. *Cancer*. 1989; 64: 1700–7.
57. Wang Q, Zhong YJ, Yuan JP, Shao LH, Zhang J, Tang L, Liu SP, Hong YP, Firestone RA, Li Y. *J Transl Med*. 2013; 11: 1.